SANDIA REPORT

SAND2016-0216
Unlimited Release
Printed January 2016

SWiFT Site Atmospheric Characterization

Christopher L. Kelley, Brandon L. Ennis

Prepared by
Sandia National Laboratories
Albuquerque, New Mexico 87185 and Livermore, California 94550

Sandia National Laboratories is a multi-program laboratory managed and operated by Sandia Corporation, a wholly owned subsidiary of Lockheed Martin Corporation, for the U.S. Department of Energy's National Nuclear Security Administration under contract DE-AC04-94AL85000.

Sandia National Laboratories

Issued by Sandia National Laboratories, operated for the United States Department of Energy by Sandia Corporation.

Available to DOE and DOE contractors from
U.S. Department of Energy
Office of Scientific and Technical Information
P.O. Box 62
Oak Ridge, TN 37831

Telephone: (865) 576-8401
Facsimile: (865) 576-5728
E-Mail: reports@adonis.osti.gov
Online ordering: http://www.osti.gov/bridge

Available to the public from
U.S. Department of Commerce
National Technical Information Service
5285 Port Royal Rd
Springfield, VA 22161

Telephone: (800) 553-6847
Facsimile: (703) 605-6900
E-Mail: orders@ntis.fedworld.gov
Online ordering: http://www.ntis.gov/help/ordermethods.asp?loc=7-4-0#online

SAND2016-0216
Unlimited Release
Printed January 2016

SWiFT Site Atmospheric Characterization

Christopher L. Kelley, Brandon L. Ennis
Wind Energy Technologies Department
Sandia National Laboratories
P.O. Box 5800, MS1124
Albuquerque, NM 87185

Abstract

Historical meteorological tall tower data are analyzed from the Texas Tech University 200 m tower to characterize the atmospheric trends of the Scaled Wind Farm Technologies (SWiFT) site. In this report the data are analyzed to reveal bulk atmospheric trends, temporal trends and correlations of atmospheric variables. Through this analysis for the SWiFT turbines the site International Electrotechnical Commission (IEC) classification is determined to be class III-C. Averages and distributions of atmospheric variables are shown, revealing large fluctuations and the importance of understanding the actual site trends as opposed to simply using averages. The site is significantly directional with the average wind speed from the south, and particularly so in summer and fall. Site temporal trends are analyzed from both seasonal (time of the year) to daily (hour of the day) perspectives. Atmospheric stability is seen to vary most with time of day and less with time of year. Turbulence intensity is highly correlated with stability, and typical daytime unstable conditions see double the level of turbulence intensity versus that experienced during the average stable night. Shear, veer and atmospheric stability correlations are shown, where shear and veer are both highest for stable atmospheric conditions. An analysis of the Texas Tech University tower anemometer measurements is performed which reveals the extent of the tower shadow effects and sonic tilt misalignment.

Acknowledgment

The meteorological tower data at the SWiFT site have been collected and provided by Texas Tech University's National Wind Institute. The Wind Energy Technologies Department at Sandia wishes to thank Texas Tech University for providing this high-quality historical atmospheric data set which will be invaluable for designing experiments and simulations.

Document Revisions

Date	Version	Description
12-Jan-2016	1.00	Initial release.

This page intentionally left blank.

Contents

List of Figures

List of Tables

Executive Summary

Analysis of the Texas Tech University 200 m meteorological tower has proven useful for the needs of understanding the Scaled Wind Farm Technologies (SWiFT) site atmospheric conditions and trends. The two years of data reveal trends in atmospheric conditions on the day and throughout the year which can be used to define experimental campaigns and their time of year and duration. Variation also occurs from year to year. The analysis of this two year data set produces insight, but to be more statistically accurate in the conclusions drawn it is important to include more data in the analysis. It is recommended that this analysis be updated as more data become available from the 200 m tower. The tower wake shadow is seen to affect measurements from the directional sector of 110°–155° for sensors above and including the 10.1 m (33 ft) tower station. This directional sector contains approximately 9% of the two year data set and does not correspond to any of the SWiFT turbine-turbine interaction directions $\pm$ 25°. The lower station heights, with the 2.4 m (8 ft) height used in stability calculations, have a directional blockage sector spanning 110°–170°. This range is close to the 5-diameter turbine-turbine interaction and an alternative measurement for atmospheric stability is recommended or an additional location for a 2.4 m (8 ft) station be installed.

The IEC classification of the SWiFT site is determined to be III-C from this analysis, which should be used as an input in designing or selecting rotors to be installed at SWiFT. The SWiFT turbine hub height average wind speed is 6.8 m/s and average wind direction is 176°. These averages are favorable for turbine-turbine interaction along the 5 rotor diameter spacing interaction (180° incoming wind) with turbine operation at the design point, in Region-II (up to about 8 m/s). For targeted experimental campaigns where this interaction is desired it is recommended to perform the testing over the summer or fall months, where the wind is most directional and most frequently from the south. For targeted experimental campaigns where a stable atmospheric boundary layer (ABL) is desired, this condition is most frequently found in the winter months. If unstable conditions are desired then summer months are most frequent. Neutral stability frequency, however, is not seen to be correlated with seasonal change. This analysis also reveals how the wind speed and other variable statistics change throughout the year.

Probability distributions are shown of atmospheric variables with correlation to the atmospheric stability class. For cases of high veer or shear profiles, a stable ABL is frequently required. A neutral stability with significant veer is rare. High veer cases are often associated with low turbulence intensity although data reveal cases where there is both high veer and turbulence, but are more rare. An unstable ABL most commonly has a shear exponent of 0.05 with only a small amount of spread due to the turbulent mixing caused by the surface heating. Stable conditions produce the lowest turbulence intensity, followed by near-neutral conditions and finally unstable conditions which produce the highest turbulence levels, with average levels of around 9%, 12% and 17% respectively. It is recommended to use this report to understand how the atmospheric conditions are correlated to most effectively design and perform objective experimental campaigns and simulations.

Nomenclature

DOE Department of Energy

SNL Sandia National Laboratories

SWiFT Scaled Wind Farm Technology experimental wind farm facility

A2e Atmosphere to Electrons

TTU Texas Tech University

NWI National Wind Institute

U_∞ 10 min average wind speed

θ 10 min average wind direction

TI turbulence intensity

x vector set of a quantity

$< x >$ time averaged quantity

x' turbulent fluctuating quantity

$< x_i' x_j' >$ Reynold's shear stress

NaN not a number

$(U_{north}, V_{west}, W_{vert})$ processed cardinal direction coordinate system

(U_s, V_s, W_{vert}) streamwise coordinate system aligned with the mean flow direction

θ_γ wind direction of sonic tilt misalignment plane

γ sonic tilt misalignment angle

σ_{U_∞} standard deviation of the instantaneous wind speed

TKE turbulent kinetic energy

$\theta(z)$ potential temperature

$T(z)$ 10 min average temperature

$p(z)$ 10 min average barometric pressure

$\theta_v(z)$ virtual potential temperature

$RH(z)$ 10 min average relative humidity

Ri_B Bulk Richardson number

α power law velocity profile exponent

$Pr(x)$ probability of condition x

k Weibull distribution shape factor

λ Weibull distribution scale factor

$\rho(z)$ 10 min average air density

IEC International Electrotechnical Commission

V_{avg} annual average wind speed at hub height

$I_{ref@15m/s}$ expected value of hub height turbulence intensity at a 10 min average wind speed of 15 m/s

AGL above ground level

$x \cap y$ intersection of condition x and condition y

Introduction

As the scale of wind energy installations continues to grow and represent a larger portion of the energy production in the United States of America it becomes increasingly important to understand the impacts of operating wind turbines within these complex flow environments. The Scaled Wind Farm Technologies (SWiFT) facility was established to study turbine-turbine wake interactions experimentally. There are many features of waked operation of a wind turbine, including reduced power and increased loads, which are all a function of turbine spacing and atmospheric conditions. The following analysis of the atmospheric conditions at the SWiFT site has been performed to be used as a tool to inform and design experimental campaigns. This analysis provides approximate conclusions about how frequent and the magnitude of atmospheric conditions of importance to wind energy. The analysis also enables modelers to simulate the site using probable conditions in advance of experimental campaigns knowing that these conditions are likely to occur.

The Department of Energy (DOE) Atmosphere to Electron (A2e) program is an effort coordinating DOE wind energy research programs around those relevant to the wind farm as opposed to a single turbine. This program includes thrust areas which trace the energy and forces from the atmosphere all the way to the electrical lines. A major part of this research involves improving the physics understanding of the wake and rotor performance in waked operation and to use that to improve high-fidelity wind farm models. This has been planned to be carried out through a formal verification and validation (V&V) campaign, performed in part at SWiFT. Planning for that campaign and understanding the availability of cases with atmospheric conditions relevant to different sites is important in development of the overall V&V plan.

In addition to wind farm performance being affected by the wakes within the boundaries, there is also need for understanding of large flow variations arising from the atmospheric forcing. The DOE A2e Mesoscale-Microscale Coupling (MMC) project was established to understand the how well and under what conditions the power of a wind farm can be ultimately forecasted in advance of knowledge of wind conditions through mesoscale modeling of the regional atmosphere. This predictive capability would allow utility companies to ramp the more efficient power generation systems in advance of the change in energy provided from the wind, making wind energy a more grid-friendly renewable power source. The first year of the MMC project research has been performed using the SWiFT site historical data and this type of research is another motivation for the atmospheric characterization analysis.

This page intentionally left blank.

Chapter 1

Scaled Wind Farm Technologies Site Background

1.1 Scaled Wind Farm Technologies Site Description

The DOE/SNL Scaled Wind Farm Technology (SWiFT) facility was established for research and development in support of the DOE Wind Energy Program. SWiFT also serves the interests of the private and public sectors; such as universities, industry and other national laboratories. The development of the SWiFT facility was done in partnership between DOE, SNL, Vestas Wind Systems, Texas Tech University's National Wind Institute (NWI) and Group NIRE. The SWiFT facility is located in Lubbock, Texas within the Reese Technology Center which houses many of the NWI facilities. A picture of SWiFT showing its relation to some of the TTU atmospheric facilities is shown in Figure 1.1.

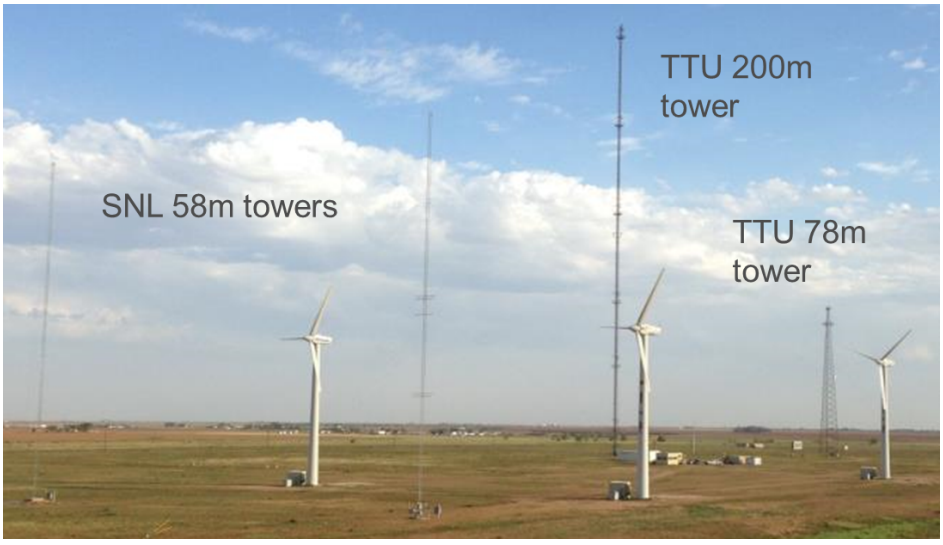

Figure 1.1. SWiFT Facility with Adjacent Meteorological Towers.

This location was chosen to house the SWiFT facility due to its excellent wind resource, flat

terrain and the partnership with Texas Tech University. The SWiFT site is within the Southern Great Plains with a surrounding landscape of grassland with small bushes, providing a low surface roughness which enables low turbulence levels. The adjacent NWI facilities includes a 200 m meteorological tower which logs high-resolution data, a 78 m tower with 10 min averaged data, a radar profiler with 20 min logs of wind speed, direction, and a virtual temperature up to 6 km in the atmospheric boundary layer, along with surrounding and nearby sodar and weather station networks.

The SWiFT experimental wind farm consists of three reconfigured Vestas V27 turbines in a 3-5-6 diameter spacing array with two dominantly upstream 58 m meteorological towers. These machines have a hub height of 32.5 m and original equipment manufacturer (OEM) rotor diameter of 27 m, meaning the rotor spans 19-46 m vertically. The turbine-turbine interaction with a 5 diameter is exactly aligned for a 180°/0° incoming wind, from the south. The turbine-turbine interactions with 6 diameter and 3 diameter spacing's are exactly aligned at 210°/30° and 266°/86°. Further details about the SWiFT facility can be found in Reference [4].

1.2 Texas Tech University 200 m Tower Data Acquisition

The data used in this analysis were acquired by Texas Tech University (TTU) using their 200 m meteorological tower beginning June 23, 2012 and ending December 31, 2014. This data set includes 731 days of high quality data containing the complete measurement package.

1.2.1 Texas Tech University 200 m Tower History

The 200 m meteorological tower operated by TTU's National Wind Institute is the cornerstone facility at the Reese Technology Center, where the SWiFT site is co-located. This tower was originally erected in the year 2000 and has undergone multiple iterations of hardware, software and instrumentation upgrades which have resulted in years of high quality data and the current configuration. The tower was installed by TTU to study extreme wind events which primarily arise from the West and South-West. More information is provided regarding the TTU 200 m meteorological tower by Hirth and Schroeder [1].

1.2.2 Texas Tech University 200 m Tower Description

The TTU 200 m tower provides measurements of 3-d velocity, temperature, barometric pressure, and relative humidity at 10 vertical stations. The sensors used and station location are shown in Tables 1.1 and 1.2. The sensor channel names and measurement units provided from TTU are summarized in Table 1.1. TTU also processes the velocity measurements to cardinal directions as part of their data archiving, with naming convention shown. The data acquisition takes place as four distinct sensor groups spanning the ten station heights. The measurement stations have

the full set of instrumentation except for the two lowest tower heights, 0.9 and 2.4 m (3 and 8 ft), which do not include a propeller anemometer.

Table 1.1. TTU 200 m Tower Station Measurement Package.

Sensor	TTU Raw Channels	[units]	TTU Processed Channels
3d Sonic Anemometer	*SonicU_NNft*	mph	*Sonic_North_NNft*
	SonicV_NNft	mph	*Sonic_West_NNft*
	SonicW_NNft	mph	*Sonic_Vert_NNft*
	SonicT_NNft	deg F	
Temperature	*Temp_NNft*	deg F	
Relative Humidity	*RH_NNft*	$[0:100]\%$	
Barometric Pressure	*BP_NNFt*	in Hg	
Propeller Anemometer[1]	*U_NNft*	mph	*UVW_North_NNft*
	V_NNft	mph	*UVW_West_NNft*
	W_NNft	mph	*UVW_Vert_NNft*

[1]Propeller anemometers are not mounted at the two lowest tower heights; (3,8) ft

Table 1.2. TTU 200 m Tower Station Measurement Package.

Sensor Group	1			2			3			4
Height [m]	0.9	2.4	4.0	10.1	16.8	47.3	74.7	116.5	158.2	200.0
Height [ft]	3	8	13	33	55	155	245	382	519	656
Sensor Package	partial[1]	partial	full	full	full	full	full	full	full	full

[1]Partial sensor package includes all but the propeller anemometers in Table 1.1.

A schematic of the 200 m tower and sensor mounting location and orientation is shown in Figure 1.2. This figure illustrates the relative sensor location and the orientation of the full sensor package. The sensors are all mounted on a boom arm that extends 14 ft away from the tower structure, which has an equilateral triangular cross-section with 4 ft sides. The measurement boom arms are mounted nominally at 300° clockwise from North. Accurate measurements of the precise mounting angle are recorded for each vertical station boom arm and are used for the TTU processing of the anemometers to the cardinal directions.

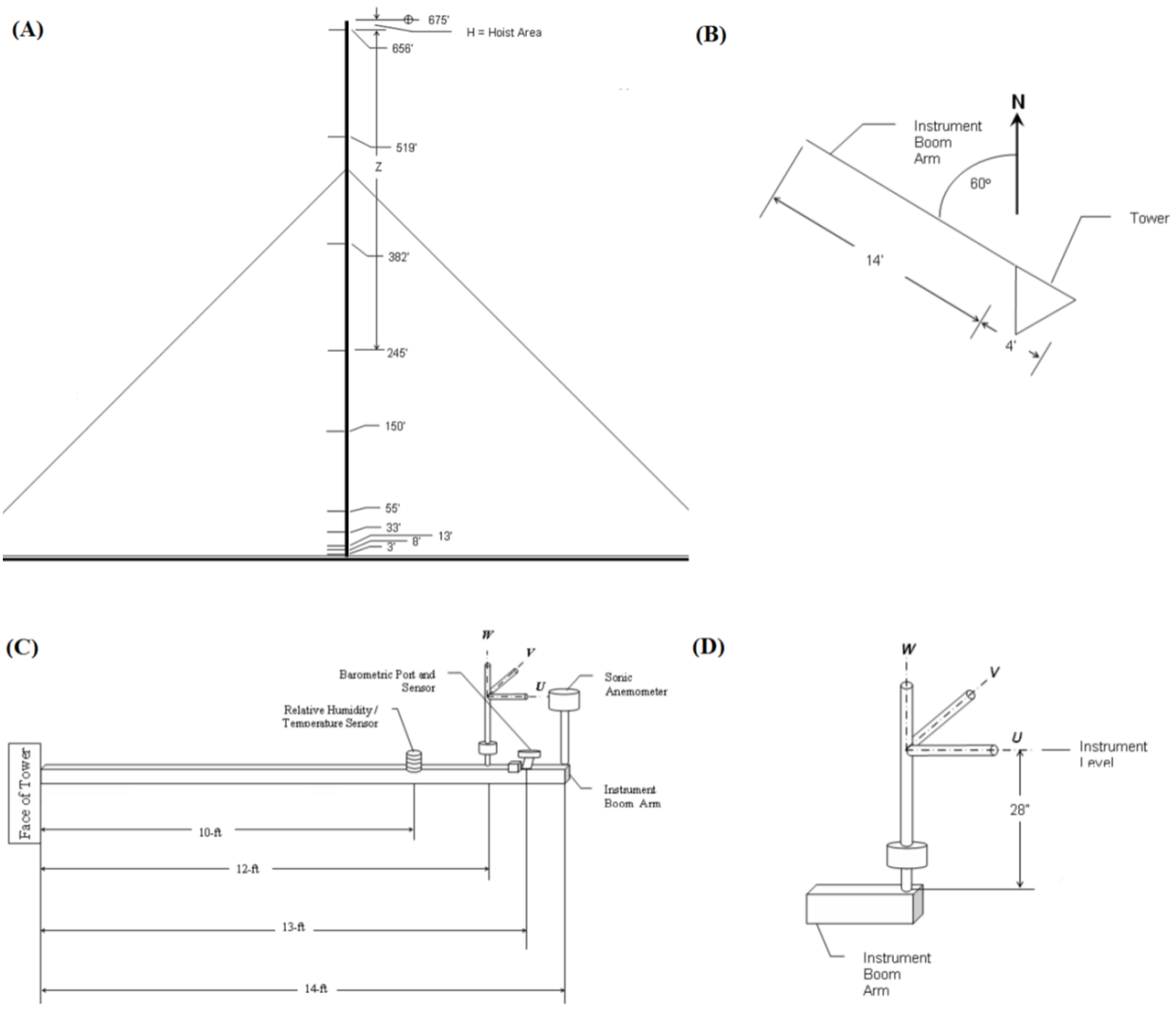

Figure 1.2. Texas Tech University 200 m Meteorological Tower Dimensions [1].

Chapter 2

Data Analysis Methods for the Texas Tech University 200 m Tower

2.1 Data Filtering and Corrections

The 200 m tower data are processed by TTU to provide measurement values in engineering units and velocities with a coordinate system aligned with cardinal directions. Additional processing and data filtering is performed to ensure that only accurate measurements are used in the following analysis by performing quality checks and removing data where values are affected by the tower structure.

2.1.1 Data Quality Check Methods

Data are quality checked prior to the analysis of site atmospheric characteristics. Artificial values in experimental measurements can arise from voltage spikes in the data acquisition system, excessive particulate passing through the sonic anemometer transducer path, among other possible sources. Where data points from the 50 hz samples are identified to be incorrect they are replaced with a "not a number" identifier, *NaN*. In the calculation of time averaged statistics functions are used which ignore the 50 hz *NaN* signals whose value has been identified as unrealistic.

Measurement Bounds Check

The first test for data quality is on the absolute measurement magnitude, that it is within bounds for the site and for the instrumentation. This check serves to remove obviously erroneous values which could affect the success of additional quality checks.

Spike Detection

Spikes are statistical outliers in the time series data and are identified using a Median Absolute Deviation (MAD) definition. The MAD is the median of the time series data deviation from the

median of the time series j, as described in Equations 2.1-2.2. A spike then is detected when a data point's deviation from the median of the time series is greater than an integer number of MAD's scaled by a constant, K, determined from the assumed distribution, as described in Equation 2.3. The scaling constant is $K = 1.4826$ for Gaussian distributed data and $K = 1.3037$ for Weibull distributed data.

$$\tilde{X}_j = median\{x_i\} \tag{2.1}$$

$$MAD_j = median\{|x_i - \tilde{X}_j|\} \tag{2.2}$$

$$|x_i - \tilde{X}_j| > n \cdot K \cdot MAD_j \tag{2.3}$$

In this analysis a time window of 5 min was chosen using a scaling constant for Gaussian distributed data and with a spike defined where $n = 5$.

Hold Detection

An additional data quality test is to identify sensor signal holds. A hold is an interval in the time series data where a constant value is returned in consecutive readings, which may be indicative of a non-responsive instrument or data transmission issues. The method for detecting holds in the despiked data is using a running window of frequency distributions. Definition of n evenly-spaced frequency bins of width δx are made for consecutive, non-overlapping windows of measurement data. A hold is detected where m consecutive readings fall into the same frequency bin. The number of bins is chosen such that δx is smaller than the resolution of the data acquisition system and therefore represents a constant instrument output.

$$\delta x = \frac{max\{x_i\} - min\{x_i\}}{n} \tag{2.4}$$

Additional Quality Check

In addition to the standard quality check methods discussed, a method was needed to remove sonic anemometer data in which the signal was bouncing at a high frequency. These data showed up as high wind speed averages but were not removed by the spike detection because the median absolute deviation was large due to the high frequency of occurrence within the averaging window. These data had both an unrealistically high wind speed and high variance of wind speed. A sample plot showing 10 min averages of all of the tower heights for a 1 week time history where this error occurred is shown in Figure 2.1. As identified for this particular data set, data are considered

unrealistic and replaced with *NaN* where the wind speed mean of a 10 min data set is greater than 30 m/s or the standard deviation is above 6.75 m/s.

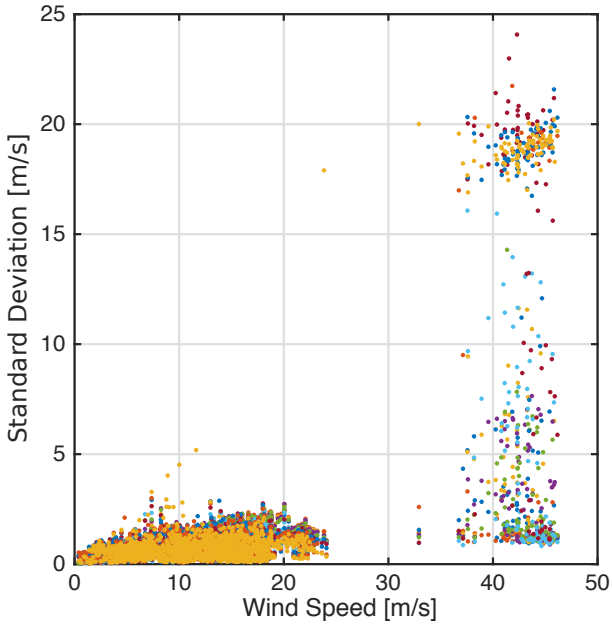

Figure 2.1. Signal Bouncing Quality Check.

2.1.2 Wind Direction Filtering

Upper Tower Height Stations (10–200 m)

Data filtering needs to be performed to account for the influence of the tower structure on the velocity measurements. The TTU 200 m tower has one boom arm at each station height mounted on the west-northwest side of the tower, as shown in Figure 1.2. For the heights of interest of this analysis, covering the SWiFT rotor area, the booms were measured to be mounted at 303° by TTU. Using the tower dimensions the tower structure width directly aligns with the sonic anemometer between approximately 123°–135°. The upstream frontal projection area of the tower changes with wind direction, and means that the sonic anemometer is between 3.5 and 4 "diameters" downstream from the tower obstruction. The wake behind the tower will expand from these geometric dimensions and cannot be determined directly since there is only one directional boom at each station. The influence of the tower wake will be to decrease wind speed and increase turbulence, meaning the effect would be expected to be most noticeable in the turbulence intensity (TI). As an attempt to remove the dependency of the actual turbulence intensity magnitude with wind direction the comparison will first be made looking only at cases with a neutral atmospheric stability, where a more consistent magnitude would be expected. This comparison is shown in Figure 2.2 for the measurement heights near the SWiFT rotor bottom and top, for cases where the wind speed at

16.8 m (55 ft) is greater than 3 m/s. The geometric width of the tower, in degrees, is shown with the two vertical black lines, when the tower structure is upstream of the anemometer.

From Figure 2.2 a clear increase in turbulence intensity is observed in the region where the sonic anemometer is waked by the tower. The tower wake width is expected to be larger in regards to the effect on turbulence than the produced velocity deficit. In the wake's shear layer the velocity deficit recovers more quickly with distance than for turbulence effects. While the velocity deficit is recovering towards the wake centerline the turbulence in the shear layer is spreading. It is likely for this tower that the wake's effect on average velocity measurements is a narrower directional sector than for turbulence characterization, but this analysis is to determine the width of the tower wake in terms of affecting turbulence quantities. The plot of turbulence intensity versus wind direction for the neutral stability cases reveals the sector of disturbed flow caused by the tower structure. The tower shadow directional sector is identified as occurring between 110°–155° at the SWiFT rotor heights, as indicated by the red box.

Another way of identifying and confirming the directional sector to remove is performed by looking at the time average of the streamwise horizontal plane Reynold's shear stress, $< u_s' v_s' >$, versus wind direction. These data are plotted in Figure 2.3 for the SWiFT rotor top height, with a similar observation at the 16.8 m (55 ft) rotor bottom station. The Reynold's shear is a noisier quantity than turbulence intensity, but is additionally helpful in confirming the directional sector to remove. The Reynold's shear is nominally zero when there is nothing disturbing the atmospheric flow, although it is not always zero due to atmospheric vortices which are a result of shear in the freestream. A net positive streamwise Reynold's shear is seen as the wind direction moves southward towards the tower. This time average Reynold's shear in the streamwise coordinate system can be understood as a net momentum transfer moving towards the centerline of the wake. Where the Reynold's shear crosses the axis at around 133° is best identified as the wake center, although it is clearly not a symmetric wake due to the asymmetric tower structure's appearance to the flow in this orientation. This wake centerline is about 4° higher than the geometric center of the tower structure of 129°, due to the flow asymmetry. For the neutral stability cases, the Reynold's shear is seen to return to its nominal behavior before reaching the bounds of the 110°–155° directional sector.

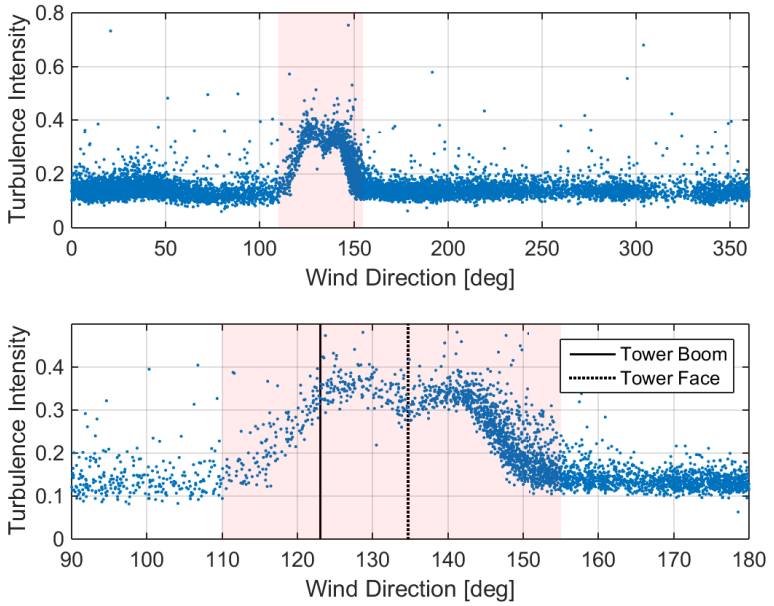

(a) 16.8 m (55 ft) Tower Height

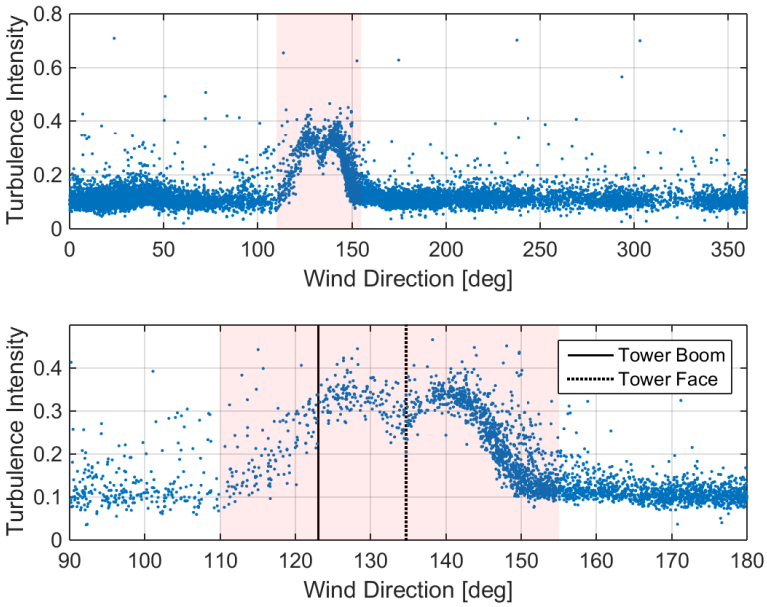

(b) 47.3 m (155 ft) Tower Height

Figure 2.2. Turbulence Intensity vs. Wind Direction for all Neutral Stability Cases.

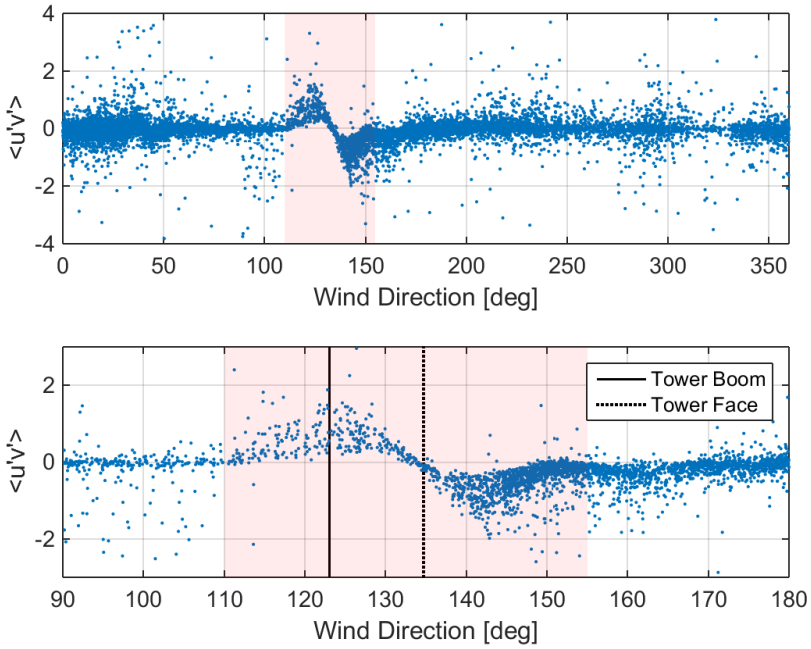

Figure 2.3. Streamwise Horizontal Plane Reynold's Shear vs. Wind Direction Comparison at 47.3 m (155 ft) Tower Height, Neutral Atmospheric Stability.

The previous analysis included data from only neutral cases, as these cases are most consistent and easiest to draw conclusions from. It is important also to understand the effect of the tower wake for stable and convective atmospheric stability conditions. The expectation is that for cases where there is a higher TI there will be a correspondingly larger wake width. Figure 2.4 shows TI versus wind direction for stable and convective cases. The stable case in Figure 2.4(a) reveals a wake width that is within the chosen tower wake direction sector by about $\pm 5^{\circ}$, which can be explained by the lower average TI than for the neutral cases. The convective cases in Figure 2.4(b) reveal the highest TI as would be expected for these flow conditions with high mixing. The scatter in TI for the convective cases makes it more difficult to identify the tower wake width. There is a sector where low TI values are not present in the data which is a result of the effect of the tower on the flow. Comparison of this region of increased TI with the selected 110°–155° tower wake sector reveals good agreement between the two regions, where at the bounds of the tower wake sector the TI appears to return to the average scatter existent in the non-waked sector.

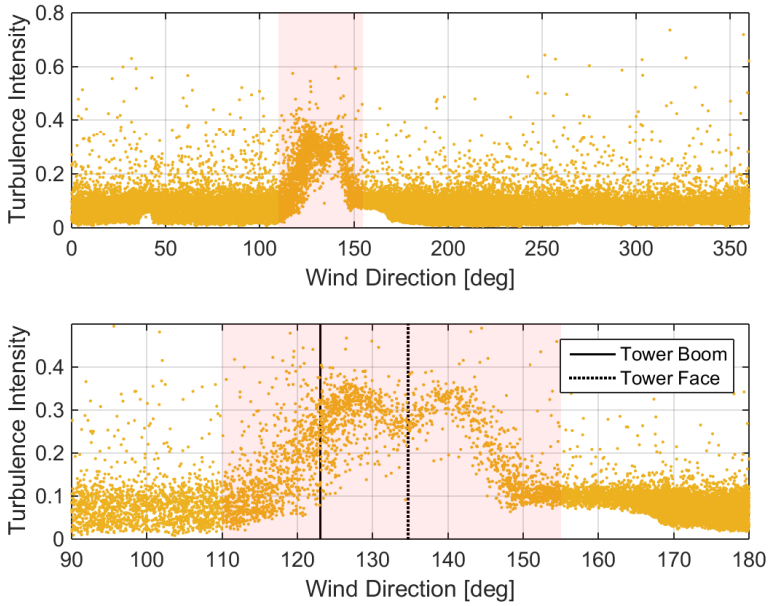

(a) Stable Atmospheric Stability

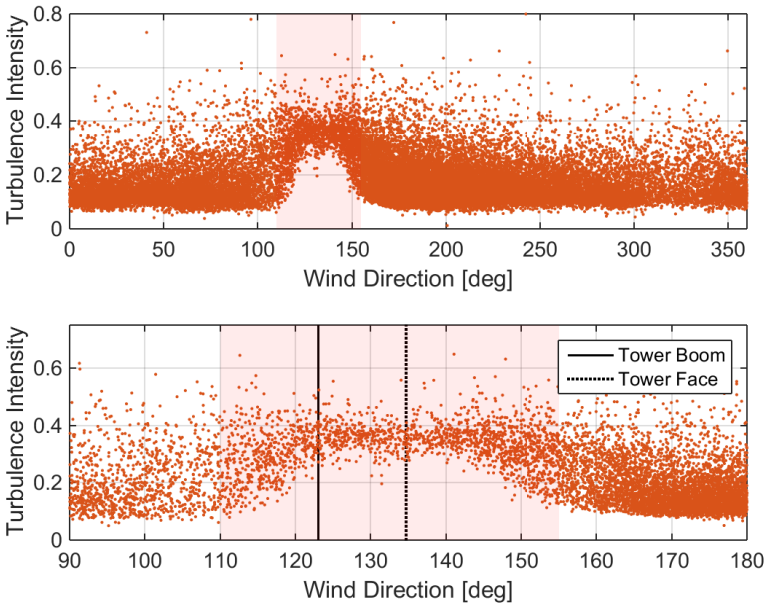

(b) Convective Atmospheric Stability

Figure 2.4. Turbulence Intensity vs. Wind Direction Comparison at 47.3 m (155 ft) Tower Height.

The streamwise horizontal plane Reynold's shear is also shown for the stable and convective atmospheric stability data in Figure 2.5, for completeness. The stable data again agree with the selected tower wake direction sector identified conclusively. It is difficult to draw an exact conclusion from Figure 2.5(b) for the convective data because there is so much scatter in this quantity and variation in this stability case with wind direction in even the obviously non-waked sectors. The variation in the non-waked sector even has a greater magnitude than the value of the Reynold's shear present when there is momentum recovery caused by the tower which makes this analysis additionally difficult. Ideally, the width of the tower wake would be defined where the net streamwise Reynold's shear returns to an average of zero. This is observed at 110°, but on the southern side of the wake if you followed this requirement then you would define the tower wake to extend to approximately 180° which would mean the wake was extremely asymmetric and also doesn't agree with the result from looking at TI. Due to the difficulty in using the convective cases to define the wake width, and from the conclusiveness of the neutral and stable cases, the wind direction sector defining the tower wake at the relevant SWiFT rotor heights is kept at 110°–155°.

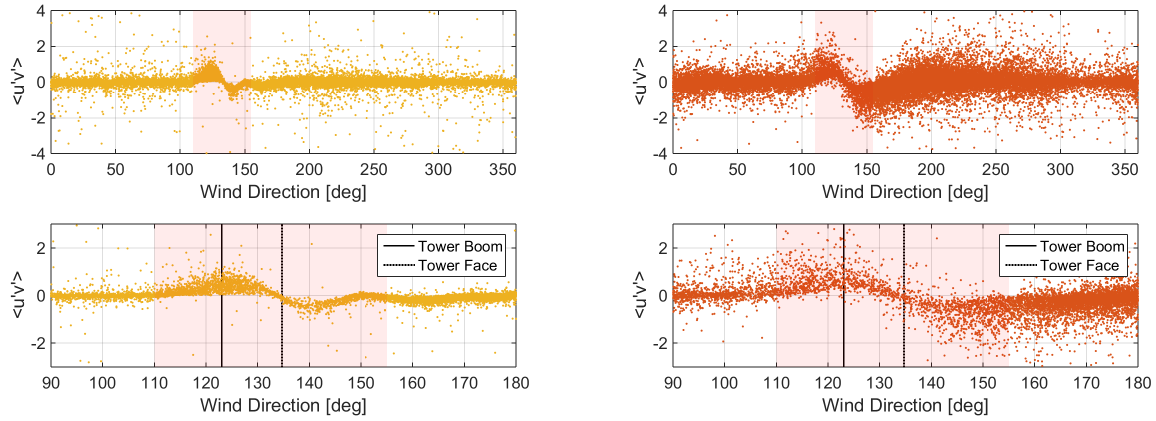

(a) Stable Atmospheric Stability

(b) Convective Atmospheric Stability

Figure 2.5. Streamwise Horizontal Plane Reynold's Shear vs. Wind Direction Comparison at 47.3 m (155 ft) Tower Height.

Lowest Tower Height Stations (0.9–4 m)

The calculation to determine atmospheric stability does not use the rotor height sensors, but is instead calculated using the 2.4 m (8 ft) and 10.1 m (33 ft) sensors. The 10.1 m (33 ft) sensor has the same mounting and tower geometry as the SWiFT rotor height sensors, with the same tower wake structure as previously shown. The 2.4 m (8 ft) sensor is not expected to behave the same as the higher sensors since it is mounted differently and because the tower structure is different at this height due to additional power boxes and tower access structures, as shown in Figure 2.6. In addition to these differences the turbulence as measured by the 2.4 m (8 ft) sensor is likely affected by a 1-story test building upstream of the tower from the southeast, shown in

Figure 2.6(c). The same analysis as above is therefore needed for the 2.4 m (8 ft) sensor before the stability calculations should be trusted.

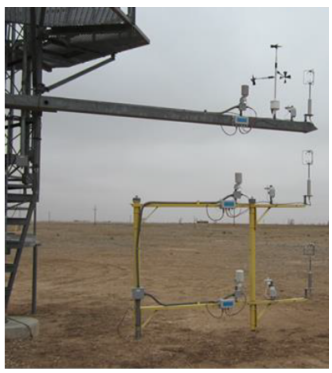

(a) Sensor Mounting at 0.9, 2.4 and 4 m (3, 8 and 13 ft).

(b) Tower Structure Near the Ground.

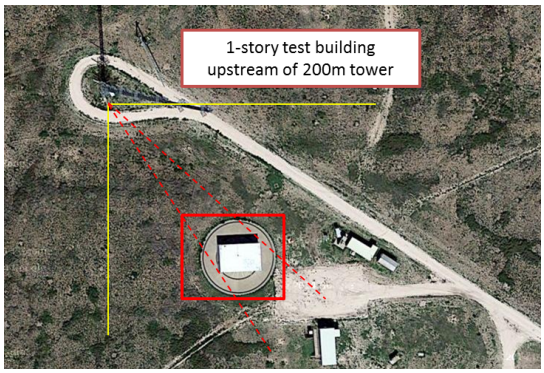

(c) Adjacent Structures to the 200 m Tower.

Figure 2.6. TTU 200 m Tower Lower Height Sensor Mounting and Obstructions [1].

Through observation of the turbulence intensity and streamwise Reynold's shear stress the tower wake width is defined for the 2.4 m (8 ft) sensor. These plots, for the separated atmospheric stability conditions, are shown in Figure 2.7. From this analysis the tower wake width at 2.4 m (8 ft) is selected to be 110°–170°. Width is added to the southern side of the direction sector, which is where the additional tower structures and the upstream building reside.

Tower Wake Filtering Summary

In the analysis to follow the directional sector between 110°–155° will be removed from all rotor height averages. In figures where quantities are not plotted vs. wind direction, the variables plotted are those with the tower wake wind direction sector removed. For the data analyzed in this report, removing this wind direction sector accounts for 8.7% and 9.2% of the total data set at the 16.8 and 47.3 m (55 and 155 ft) measurement heights. The stability averages and plots when not shown versus wind direction will remove the 2.4 m (8 ft) sensor waked direction sector of 110°–170°. Removing this larger sector corresponds to 15.6% of the two years of data analyzed.

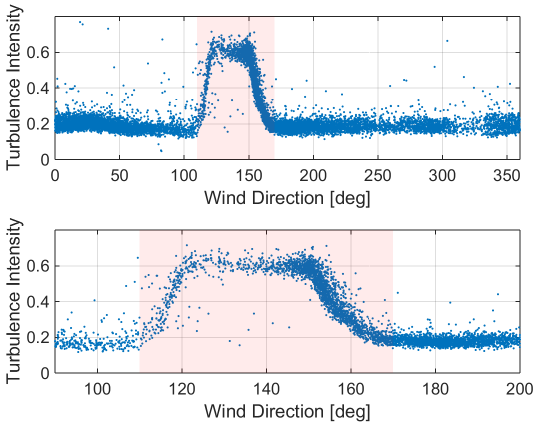

(a) Turbulence Intensity, Neutral Atmospheric Stability.

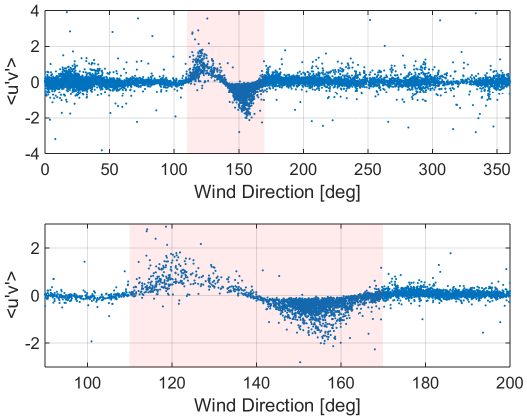

(b) Reynold's Shear, Neutral Atmospheric Stability.

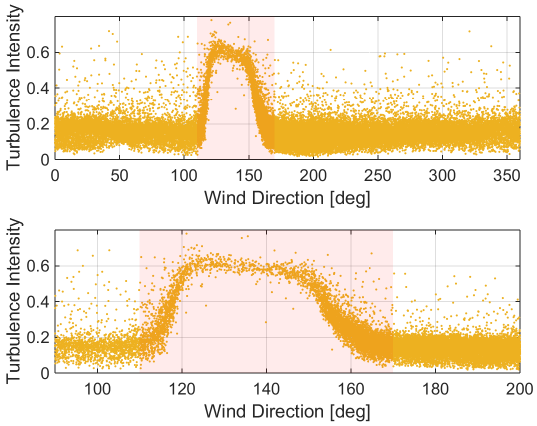

(c) Turbulence Intensity, Stable Atmospheric Stability.

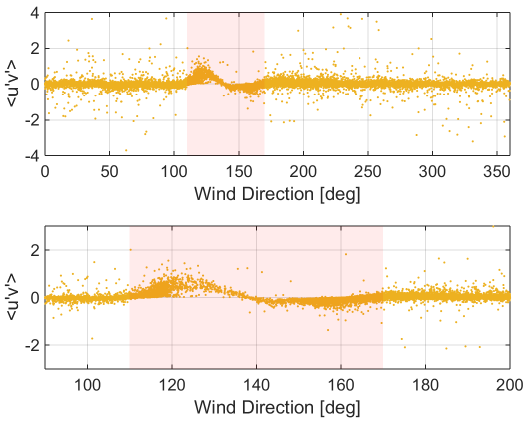

(d) Reynold's Shear, Stable Atmospheric Stability.

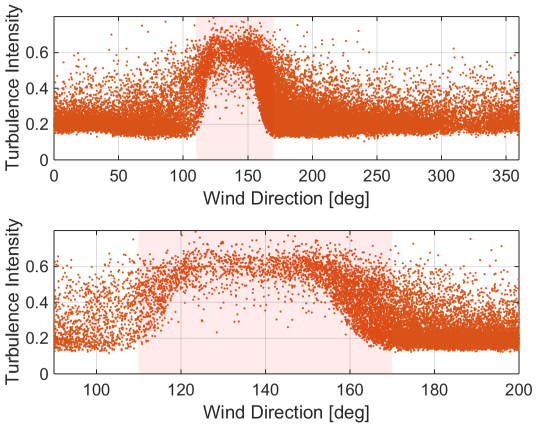

(e) Turbulence Intensity, Convective Stability.

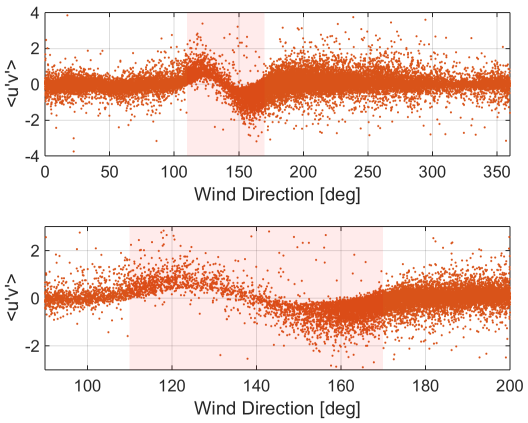

(f) Reynold's Shear, Convective Stability.

Figure 2.7. Tower Wake Direction Sector Identification for 2.4 m (8 ft) Sensor.

2.1.3 Sonic Alignment Corrections

The sonic anemometers are the primary velocity measurements used in the analysis to follow. As was shown in Figure 1.2 the velocity measurements are not initially aligned with the cardinal directions. This coordinate transformation is performed by TTU in their conversion of the raw sensor outputs to their processed values. This cardinal transformation is performed at each mounting height using precise measurements of the three rotational angles of the boom arm, the three sonic anemometer rotational angles and actual measured length of each sensor. These measurements and corrections are also made for each propeller anemometer. From these calculation, a North, West and Vertical velocity component are defined with velocity positive *from* the North and *from* the West and positive upward in a right-handed coordinate system.

This bulk alignment is very near a true North-West-Vertical coordinate system, however some of the sonic anemometers are seen to have tilt misalignment. Anemometer tilt misalignment can be detected by looking at the trend of the average vertical velocity component vs. wind direction, as shown analytically in Figure 2.8. In the presence of a tilt misalignment, under the assumption of a net average vertical velocity component of zero, there is a sinusoidal dependency noticed in the non-dimensional vertical velocity with wind direction. This is due purely to the vertical velocity sensor now including a component of the incoming horizontal-plane velocity which is a maximum along the tilt axis plane. The amplitude of the sinusoid is related to the magnitude of the tilt misalignment, as shown in Figure 2.8(b).

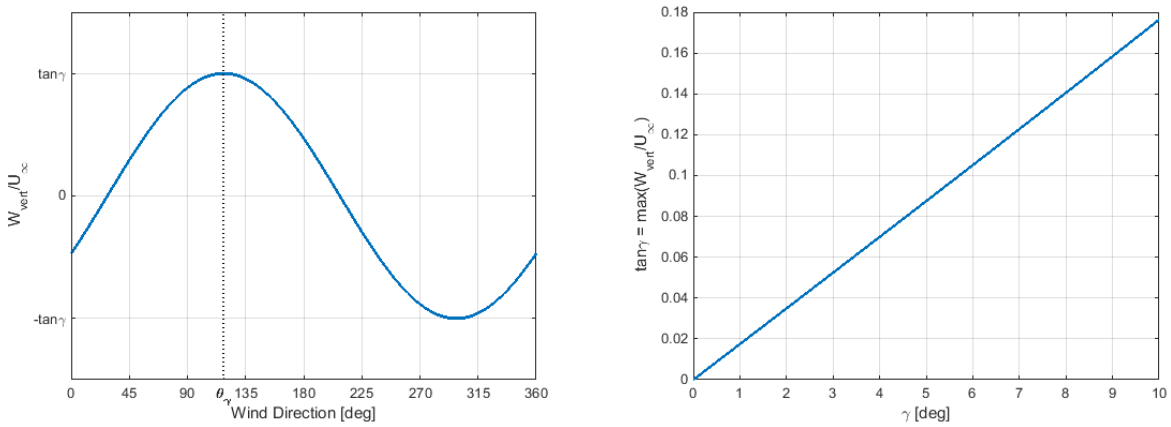

(a) Sonic Normalized Vertical Velocity with Tilt.

(b) Tilt Angle, γ, Definition.

Figure 2.8. Analytical Representation of a Sonic Anemometer with Tilt Misalignment.

Averages of the vertical velocity component for the sonic anemometer at 74.7 m (245 ft) are shown plotted vs. wind direction in Figure 2.9 for neutral stability conditions (again, to reduce the noise on the analysis). The 74.7 m (245 ft) sensor is one of the sensors with the most tilt misalignment. There is excessive scatter when not normalized by the average wind speed caused

by the relationship between these two velocities, so the normalized vertical velocity is also shown. In these figures the blue dots represent 10 min averages from the tower data, and the dashed red curve is a bin average of these data. A clear sinusoidal trend is observed in the normalized vertical velocity plot as is expected with tilt misalignment.

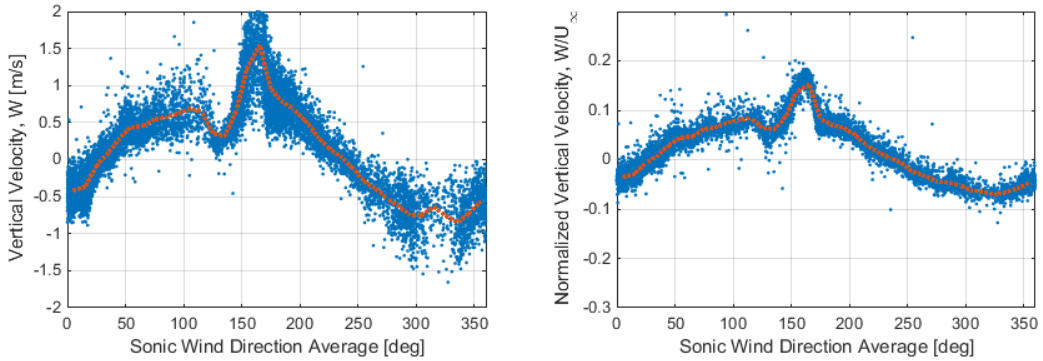

Figure 2.9. Sonic Misalignment Effect on Vertical Velocity for the Sonic at 74.7 m (245 ft). (Blue dots are 10 min average data points. Red curve is a bin average of these data.)

To correct for the sonic tilt misalignment a coordinate transformation needs to be performed on the TTU North-West-Vertical coordinates. This transformation to reduce the effect of tilt misalignment errors follows three steps. The transformation begins by a counter-clockwise rotation about the vertical (z) axis θ_γ to the tilt axis plane where the vertical velocity component is highest, as shown in Figure 2.8(a). From here a positive tilt about the west (y) axis of γ is performed to cause the original vertical axis to be truly vertical, correcting for the tilt misalignment. What remains is to rotate the north and west coordinates back to the original north and west planes of orientation, by rotating back $-\theta_\gamma$, which is approximately the correct angle when a small tilt misalignment is assumed.

The coordinate transformation procedure to correct for the sonic tilt is shown in Equations 2.5-2.8. There are two rotation matrices, R_z and R_y, which rotates to the tilt axis plane and then corrects for the tilt, respectively. After the vertical error is corrected the coordinate system is rotated back to the cardinal directions using the R_{-z} rotation matrix. This transformation process is based on the definition of θ_γ and γ shown in Figure 2.8. θ_γ is defined using a clockwise meteorological definition of wind direction, which has been corrected for in the rotation matrices R_z and R_{-z}.

$$R_z = \begin{bmatrix} cos\theta_\gamma & -sin\theta_\gamma & 0 \\ sin\theta_\gamma & cos\theta_\gamma & 0 \\ 0 & 0 & 1 \end{bmatrix} \tag{2.5}$$

$$R_y = \begin{bmatrix} cos\gamma & 0 & sin\gamma \\ 0 & 1 & 0 \\ -sin\gamma & 0 & cos\gamma \end{bmatrix} \tag{2.6}$$

$$R_{-z} = \begin{bmatrix} cos\theta_\gamma & sin\theta_\gamma & 0 \\ -sin\theta_\gamma & cos\theta_\gamma & 0 \\ 0 & 0 & 1 \end{bmatrix} \tag{2.7}$$

$$\begin{bmatrix} U_{north'} \\ V_{west'} \\ W_{vert'} \end{bmatrix} = R_{-z}\, R_y\, R_z * \begin{bmatrix} U_{north} \\ V_{west} \\ W_{vert} \end{bmatrix} \tag{2.8}$$

This coordinate transformation method is used at each height to correct to a more true North-West-Vertical coordinate system. The first step is to approximate the tilt error, γ, and θ_γ, the wind direction where the sonic is tilted directly away from the incoming wind (wind direction where the most positive vertical velocity occurs), for each measurement station. The resulting transformed data points and bin averages of the transformed data and the original data are shown in Figures 2.10-2.11. The blue dots are the transformed 10 min averaged data, the dashed red curve is a bin average of these transformed coordinate system data, and the dashed yellow curve is a bin average of the original data. Comparison of the original and transformed coordinate systems is made through comparing the bin averages, dashed yellow and red curves.

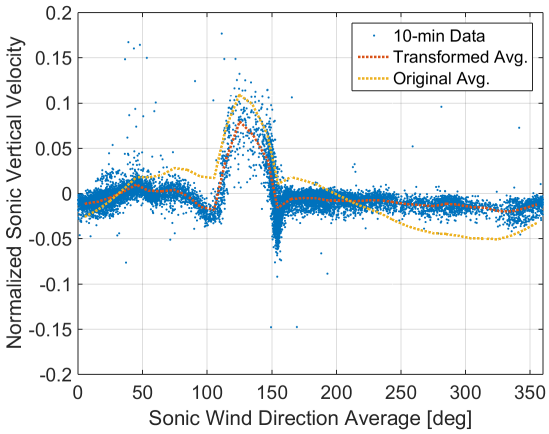

(a) Corrected Sonic Tilt, 0.9 m (3 ft).

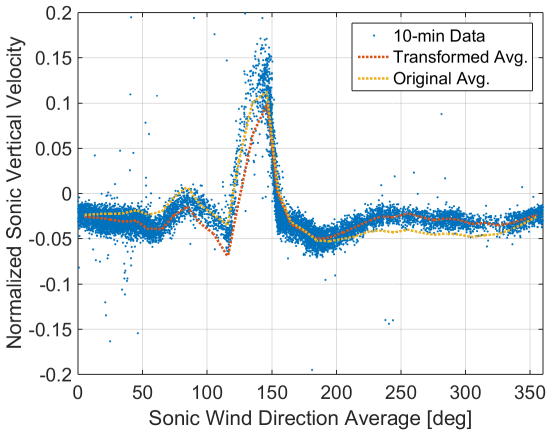

(b) Corrected Sonic Tilt, 2.4 m (8 ft).

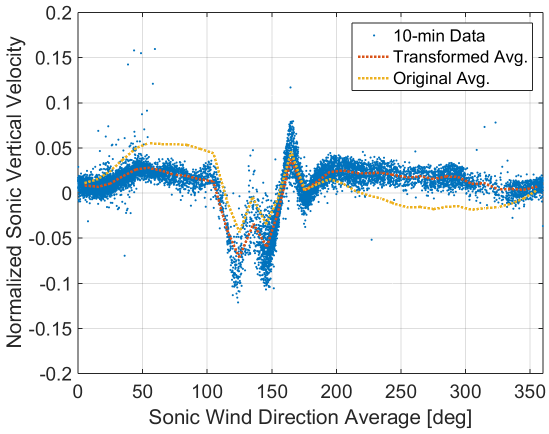

(c) Corrected Sonic Tilt, 4 m (13 ft).

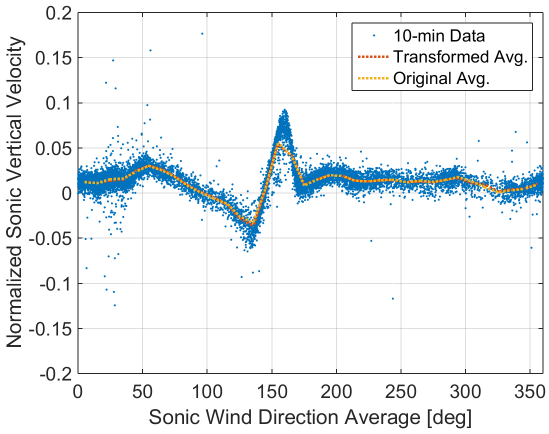

(d) Corrected Sonic Tilt, 10.1 m (33 ft).

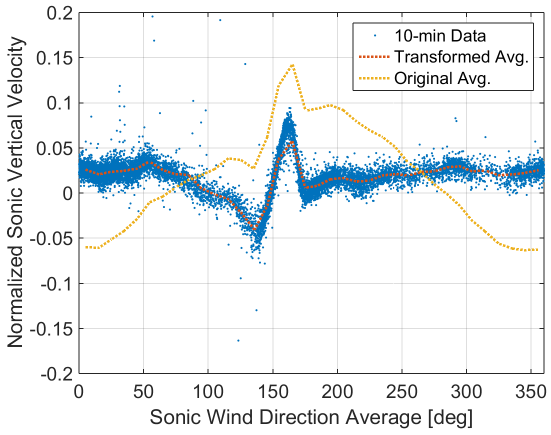

(e) Corrected Sonic Tilt, 16.8 m (55 ft).

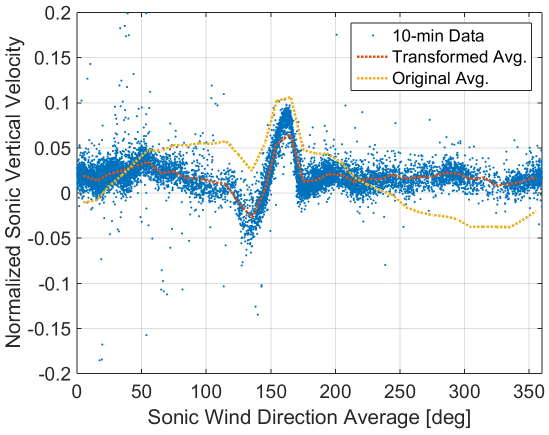

(f) Corrected Sonic Tilt, 47.3 m (155 ft).

Figure 2.10. Coordinate Transformations to Correct Tilt Misalignment, Six Bottom Heights. (Blue dots are transformed 10 min average data points. Red curve is a bin average of these data. Yellow curve is bin average of the original coordinate system data.)

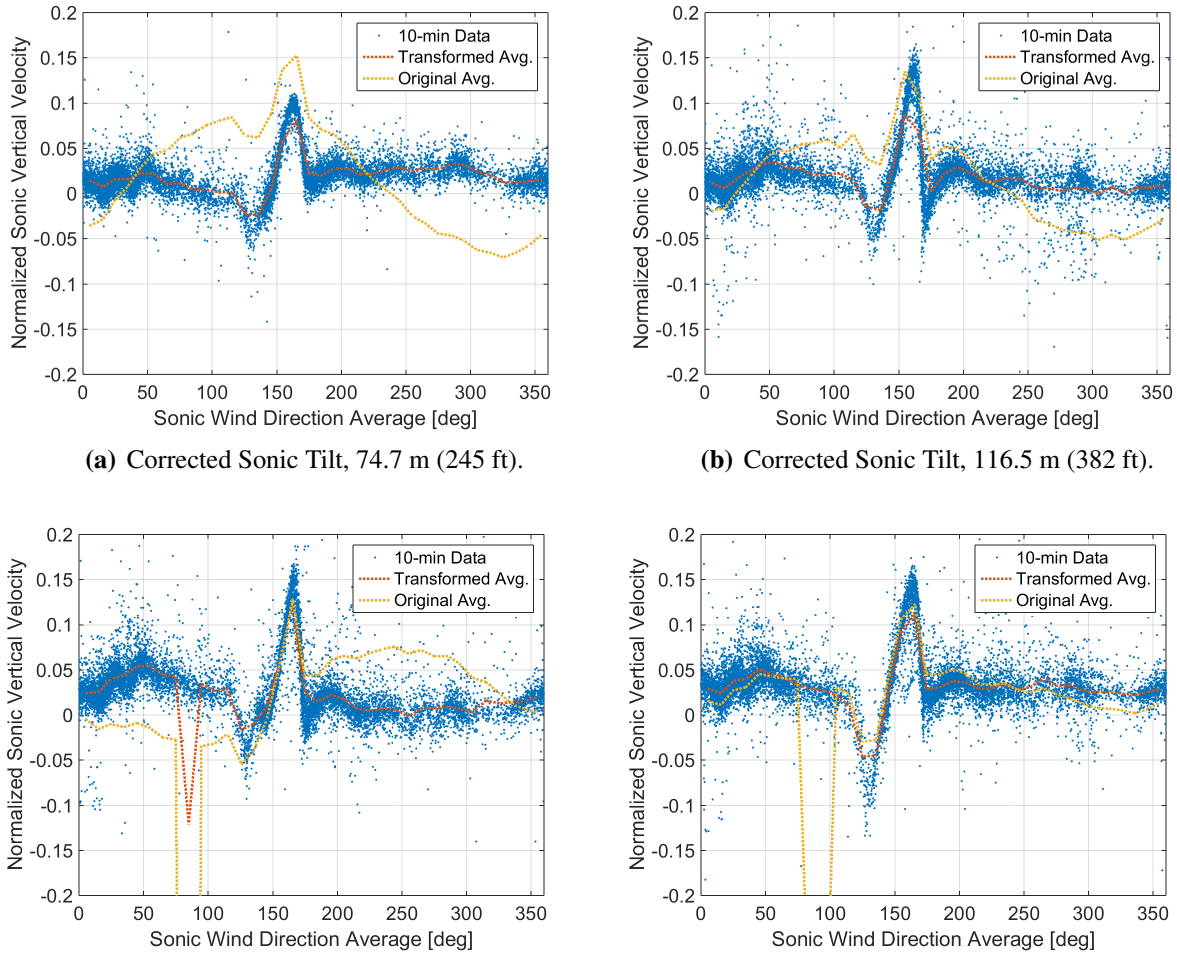

(a) Corrected Sonic Tilt, 74.7 m (245 ft).

(b) Corrected Sonic Tilt, 116.5 m (382 ft).

(c) Corrected Sonic Tilt, 158.2 m (519 ft).

(d) Corrected Sonic Tilt, 200 m (656 ft).

Figure 2.11. Coordinate Transformations to Correct Tilt Misalignment, Four Top Heights. (Blue dots are transformed 10 min average data points. Red curve is a bin average of these data. Yellow curve is bin average of the original coordinate system data.)

Correction of the sonic tilt misalignment used the transformation angles as summarized in Table 2.1. The maximum misalignment occurred at the measurement station heights 16.8 and 74.7 m (55 and 245 ft), as seen in Figures 2.10-2.11. The maximum tilt error was observed to be approximately 5° for these two stations which corresponds to a maximum normalized vertical velocity amplitude of around 0.09 as calculated in Figure 2.8(b).

The coordinate transformation is seen to improve the vertical velocity component trend to be more constant with wind direction. There is a dip followed by a spike around the sector defined by the tower wake seen at each height that deviates from the near zero average expected. The directional sector of this deviation varies from the defined sector in Section 2.1.2 which corresponds with the tower wake directional sector. The reasoning for this discrepancy in these two variables

Table 2.1. Sonic Tilt Misalignment Angles.

Height [ft]	3	8	13	33	55	155	245	382	519	656
Tilt Angle, γ	2	1	2	0	5	3	5	3	4	1
Tilt Axis, θ_γ	120	90	90	10	175	130	130	130	250	150

is currently unclear. The objective of the transformation is to get the normalized vertical velocity to be near constant with wind direction outside of the tower wake region. This constant value however is not always zero after the correction, as is the case for 0.9 and 16.8 m (3 and 55 ft) which have a near constant negative and positive value for the vertical velocity. This is likely due to instrumentation uncertainty and a bias in the sensor measurement or digital conversion.

There is an inherent scatter in the 10 min average data of around ± 0.05 normalized vertical velocity, which corresponds to approximately ± 0.5 m/s at the SWiFT rotor heights. The average vertical velocity data is not always expected to be exactly zero in the atmosphere, as shown by Ouwersloot using data from the Cabauw tower in the Netherlands [2]. Ouwersloot shows the dependency of the vertical velocity average on the averaging time at heights up to 180 m, displayed again in Figure 2.12. For the 10 min average time window used in this analysis the amount of scatter in the vertical velocity component from this data is in good agreement with Ouwersloot's results.

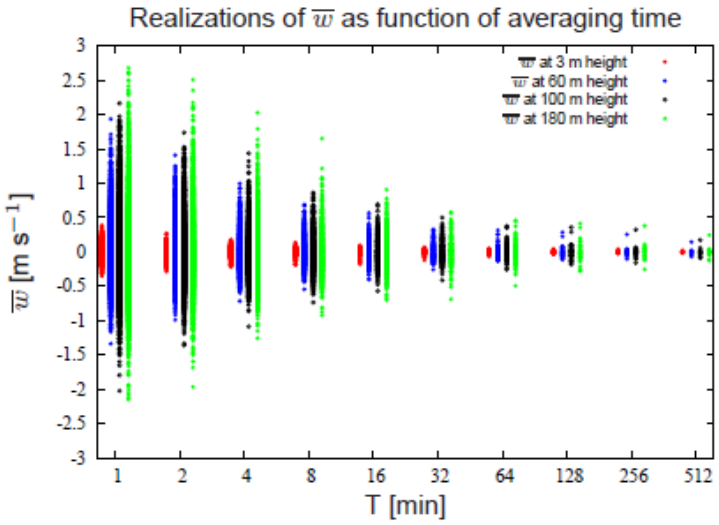

Figure 2.12. Vertical Velocity Observations using the Cabauw Tower from Ouwersloot, et al [2].

The question to answer is how much uncertainty in the measurement quantities of interest is added by this tilt misalignment. There will be a large dependency on the tilt for the variables using the vertical velocity component directly, but for quantities such as wind speed and direction

this error/uncertainty is not apparent and must be quantified. The uncertainty added to the wind speed and direction calculations depends on both the tilt angle and tilt axis location and should be calculated over the relevant range of wind speeds and directions. At low wind speeds the tilt angle has the largest effect on adding to the wind direction uncertainty, whereas at higher speeds there is a greater effect on wind speed uncertainty, dimensionally. The uncertainty added into the wind speed and wind direction measurements due to sonic tilt misalignment was determined for wind speeds relevant to wind turbine operation over the full range of wind directions. The maximum error for wind speed and wind direction is shown for each wind speed in Table 2.2 using the determined tilt angles summarized in Table 2.1. The maximum wind speed error within this range of wind speeds is 0.10 m/s, for the 5° maximum tilt error cases. Wind direction error is greatest for the lowest wind speed case and produced an uncertainty of 0.86°. These uncertainties are considered negligible to the overall measurement uncertainties. The uncertainty added to quantities which directly use the vertical velocity component can be significant, and for the purpose of this report that relates to the Bulk Richardson number representation of atmospheric stability. This value is calculated using the vertical velocity measurement from the sensors at 2.4 and 10.1 m (8 and 33 ft). From Figures 2.10(b) and 2.10(d) it is observed that these two sensor stations have little to zero tilt misalignment, and in the analysis tilt corrections of $\gamma = 1^\circ$ and $\gamma = 0^\circ$ are used, respectively. With these results it is determined that the small sonic tilt misalignments present for the TTU sensors have an insignificant effect on the presentation of the results to follow and therefore are not corrected in the analysis, but the original North-West-Vertical coordinate system as processed by TTU is used.

Table 2.2. Wind Speed and Direction Calculation Uncertainty Due to Sonic Tilt Misalignment.

Wind Speed [m/s]	Wind Speed Error [m/s]	Wind Direction Error [degrees]
3	0.055	0.86
7	0.07	0.41
10	0.08	0.31
15	0.10	0.24

2.2 Data Processing

The processes for calculating atmospheric quantities of interest to the plotting of data 10 min averages as part of this analysis are described within this section.

2.2.1 Data Variable Calculations

Wind Speed

Wind speed is defined as a horizontal wind speed, using the orthogonal wind components in the horizontal plane as shown in Equation 2.9. The average wind speed is taken by averaging the values calculated using the high-resolution data, Equation 2.10, and not from using the average of the components which would produce a different result.

$$U_{\infty,i} = \sqrt{U_{north,i}^2 + V_{west,i}^2} \tag{2.9}$$

$$< U_\infty >= \frac{1}{N} \Sigma_{i=1}^{N} U_{\infty,i} \tag{2.10}$$

Wind Direction

The average wind direction is defined as that which produces a zero-mean cross stream flow ($< V_s >= 0$). This value is found by weighting the wind directions using the vector length, horizontal wind speed. The meteorological wind rose direction convention is used which describes the direction the wind is coming *from* with 0°, 90°, and so on for directions of wind from the North, East, etc. The wind direction is calculated using the North and West coordinates as shown in Equation 2.11.

$$tan\theta = \frac{- < V_{west} >}{< U_{north} >} \tag{2.11}$$

Streamwise Coordinates

It is common to think of the velocity in terms of streamwise coordinates which means the coordinate system is aligned with the average wind direction of the time-series. The angle of this coordinate system is defined such that the average cross-stream velocity $< V_S >= 0$. This relative angle is changing for each averaging block of data and follows the definition of that for the average wind direction, θ, in Equation 2.11. To transform the horizontal cardinal velocities into a streamwise coordinate system (U_S, V_S) the rotation matrix in Equation 2.12 is used.

$$\begin{bmatrix} U_{S,i} \\ V_{S,i} \end{bmatrix} = \begin{bmatrix} cos\theta & -sin\theta \\ sin\theta & cos\theta \end{bmatrix} \begin{bmatrix} U_{north,i} \\ V_{west,i} \end{bmatrix} \tag{2.12}$$

Similarly, the turbulence fluctuations can be calculated using either coordinate system and

transformed to the other. An example transformation from the cardinal coordinate system turbulent fluctuations to the streamwise coordinate system is shown in Equation 2.13.

$$\begin{bmatrix} u'_{S,i} \\ v'_{S,i} \end{bmatrix} = \begin{bmatrix} cos\theta & -sin\theta \\ sin\theta & cos\theta \end{bmatrix} \begin{bmatrix} u'_{north,i} \\ v'_{west,i} \end{bmatrix} \tag{2.13}$$

Turbulence Intensity

The turbulence intensity (TI) is a representation of the variation in the wind speed over a period of time. With this definition a method for representing the turbulence intensity was defined in Equation 2.14. This method calculates TI based on the fluctuation of the length of the wind speed vector, without consideration of the vector direction. This definition is often called a cup-equivalent turbulence intensity because this definition is how a cup anemometer could calculate TI [5].

$$TI = \frac{\sigma_{U_\infty}}{< U_\infty >} \tag{2.14}$$

Turbulence Characteristics

Turbulent fluctuation of the high-response sonic anemometers is calculated following the standard definition shown in Equation 2.15. The turbulent fluctuations are used to calculate the Reynold's stresses as shown in Equation 2.16. The variance and covariance using the three orthogonal velocities define the Reynold's normal stresses ($i = j$) and Reynold's shear stresses ($i \neq j$). A turbulent heat flux is also calculated as the covariance of a velocity component with the turbulent temperature fluctuation measured by the sonic anemometer. The Reynold's normal stresses are used in the definition of the turbulent kinetic energy (TKE) shown in Equation 2.17, which is the one-half the average of the sum of the normal stresses.

$$x' = \{x\} - < X > \tag{2.15}$$

$$< x'_i \, x'_j >= \frac{1}{N} \Sigma_{n=1}^{N} (x'_{i,n} \, x'_{j,n}) \tag{2.16}$$

$$TKE = \frac{0.5}{N} \Sigma_{n=1}^{N} (u'_n u'_n + v'_n v'_n + w'_n w'_n) \tag{2.17}$$

Potential Temperature

The potential temperature is the temperature that an unsaturated parcel of dry air would have if it were brought adiabatically and reversibly from its initial state to a standard pressure, p_0, typically taken as 100 kPa. The potential temperature is then defined and calculated as shown in Equation 2.18, where K is taken as 0.286.

$$\theta(z) = T(z)\left(\frac{100}{p(z)}\right)^{K} \tag{2.18}$$

Virtual Potential Temperature

The virtual potential temperature is the theoretical potential temperature of dry air that would have the same density as air of a specific moisture content. The virtual potential temperature is calculated using Equation 2.19, with intermediate calculations of Equations 2.20-2.21. The constant values specific to the SWiFT site used here are from Walter with $\varepsilon = 0.622$, $e_0 = 0.611\ kPa$ and $L/R_v = 5,423\ K$ [6].

$$\theta_v(z) = \theta(z)\left(1 + 0.61\frac{r_s * RH(z)}{100}\right) \tag{2.19}$$

$$r_s = \frac{\varepsilon * e_s}{p(z) - e_s} \tag{2.20}$$

$$e_s = e_0 * \exp\left[\frac{L}{R_v}\left(\frac{1}{273} - \frac{1}{T(z)}\right)\right] \tag{2.21}$$

Bulk Richardson Number

The Richardson number is the ratio of turbulence production due to buoyancy forces to mechanical/shear production. The Bulk Richardson number is an approximation to this and characterizes the stability of the atmosphere. When the Bulk Richardson number is positive it means that there are negative buoyant forces and the atmospheric boundary layer is stable. When the Bulk Richardson number is negative it means the opposite and signifies a convective or unstable atmospheric boundary layer. Values near zero are considered neutral or near-neutral. In this analysis, when not otherwise specified, a definition of neutral stability of $|Ri_B| < 0.02$ is used, which then defines stable and unstable boundary layers. The Bulk Richardson number is calculated as shown in Equation 2.22, using the most comparable heights to 2 and 10 m. The TTU 200 m tower has sensors at 2.4 m and 10.1 m which are used for the gradients, $\Delta x = x_{10.1\ m} - x_{2.4\ m}$, and 2.4 m sensors are used for the calculation of the virtual potential temperature, θ_v, in the denominator. The 10 min

average of each input term is used in the calculation of the Bulk Richardson number, with a value of 9.81 m/s^2 used for gravity.

$$Ri_B = \frac{g\,\Delta\theta_v\,\Delta z}{\theta_v\,(\Delta U_\infty)^2} \tag{2.22}$$

Wind Veer

Veer is a measure of vertical directional change of the wind velocity. Layers of velocity within the local atmosphere having different origins produce shear layers which result in directional change with height. In this analysis veer is described using the process in Equation 2.23 over two selected heights. For the SWiFT machines veer is described using the difference between the heights 47.3 and 16.8 m (155 and 55 ft), corresponding closely to the veer over the SWiFT rotor.

$$veer = \theta(z_{upper}) - \theta(z_{lower}) \tag{2.23}$$

Wind Shear

Wind shear is a measure of the dependency of the velocity with height within the velocity profile. In this analysis the shear is represented using the power law representation of the velocity profile as described in Equation 2.24. This formulation for the velocity profile is generally applied between 30 and 300 m. The solution for the velocity profile power coefficient, α, is done using properties of logarithms to isolate the coefficient with the outcome shown in Equation 2.25. A best-fit approximation method can be used with a set of (U_∞, z) to determine the power law coefficient which approximates as a straight line of the form $y = m\,x + b$ in a log-log scale with slope α. To cover the SWiFT rotor heights the set of $\{55, 155, 245, 382, 519\}$ ft was used in the fit for the power law coefficient, spanning 16.8-158.2 m.

$$\frac{U_\infty(z)}{U_{\infty,ref}} = \left(\frac{z}{z_{ref}}\right)^{\alpha} \tag{2.24}$$

$$\ln U_\infty(z) = \alpha \cdot \ln z - (\alpha \cdot \ln z_{ref} + \ln U_{\infty,ref}) \tag{2.25}$$

Time

Lubbock, Texas is on Central Standard Time (CST) with daylight savings. The time of day figures and calculations take this into account and convert the UTC time stamp in the data to CST but without using daylight savings, as is commonly done. The time displayed is UTC-0600 in all of the subsequent figures.

2.2.2 Averaging Methods

The historical full-resolution data sets are compared in the following analysis using 10 min bin statistics. Variables listed in Section 2.2.1 are calculated either as operations on the full resolution data sets which are then averaged together or as calculations on the 10 min averages of the input variables. The variables whose averages are calculated using statistics of the 10 min data points as equation inputs are turbulence intensity, Bulk Richardson number, wind veer and wind shear. The remaining variables are calculated using the full resolution data and then averaged.

2.2.3 Plotting Summary

The plots and calculations shown in this analysis are filtered as follows, unless otherwise specified:

- Wind speed averages include only the turbine operational range, $[3, 20]$ m/s
- Wind direction sectors of 110°–155° are removed due to tower shadow for all sensors above and including 10.1 m (33 ft)
- Wind direction sectors of 110°–170° are removed due to tower shadow for all sensors below 10.1 m (33 ft)
- Atmospheric stability classes are defined around the near-neutral definition of the Bulk Richardson number $|Ri_B| < 0.02$
- The time displayed is a local time without including daylight savings, UTC-0600
- Sonic anemometer figures are shown without correcting for the tilt misalignment

Chapter 3

Historical Atmospheric Trends at the Scaled Wind Farm Technologies Site

This section presents average atmospheric conditions data collected between June 23, 2012 and December 31, 2014. This range does not begin and end at the same time of year, however, by including as much data as available more accurate monthly averages are presented for the SWiFT site due to the annual differences in weather. The sector of the wind rose from 110°–155° puts the sonic anemometer in the wake of the meteorological tower and data points falling in this sector have been removed unless plotting versus wind direction. A red shading is added onto figures representing this tower wake region when plotted. In many figures the wind data are filtered to include only those where the average is within the SWiFT turbine operational range, 3 to 20 m/s. In the following section when this filter is used it will be stated in the figure caption. Other plotting definitions and operations are summarized in Section 2.2.3.

3.1 Bulk Atmospheric Conditions

The average wind speed at all tower heights was calculated using both the sonic and propeller anemometers with the average atmospheric boundary layer profile presented in Figure 3.1. Overall there is good agreement between the two sensors except at 158 m above the ground. The propeller anemometer may produce low averages by about 0.5 m/s at this height based on the smoothness of the sonic anemometer's velocity profile. The remaining velocity and turbulence measurements presented in this analysis will use only the sonic anemometers.

The SWiFT turbine hub height, 32.5 m, is of particular importance for the inflow characterization analysis. As shown in Table 1.2 there is not a measurement station on the 200 m tower at the SWiFT hub height. The quantities shown are all for the SWiFT hub height through interpolation from the 10 min average profiles at the 16.8 and 47.3 m stations (55 and 155 ft).

The wind speed tends to have a probability that is fit well by a Weibull distribution. This fit at hub height is presented in Figure 3.2 and has the form shown in Equation 3.1. The Weibull fit produced the parameters $k = 2.773$ and $\lambda = 7.499$. The measured mean wind speed for the SWiFT turbine height is 6.82 m/s, whereas the Weibull fit estimated mean is 6.68 m/s.

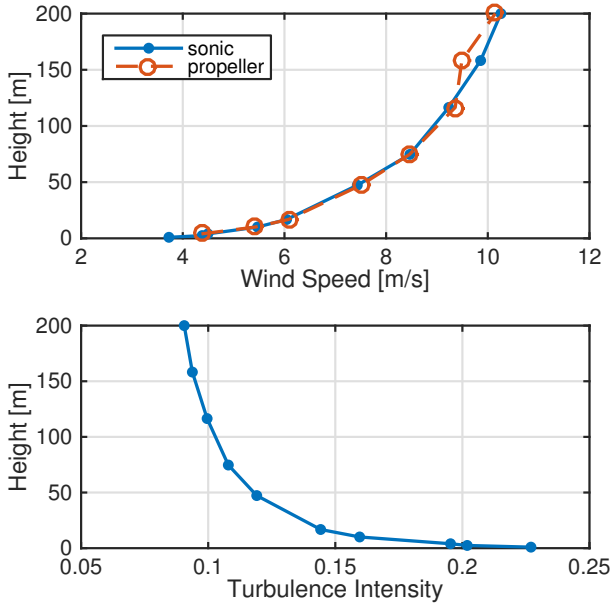

Figure 3.1. Average boundary layer profile at SWiFT.

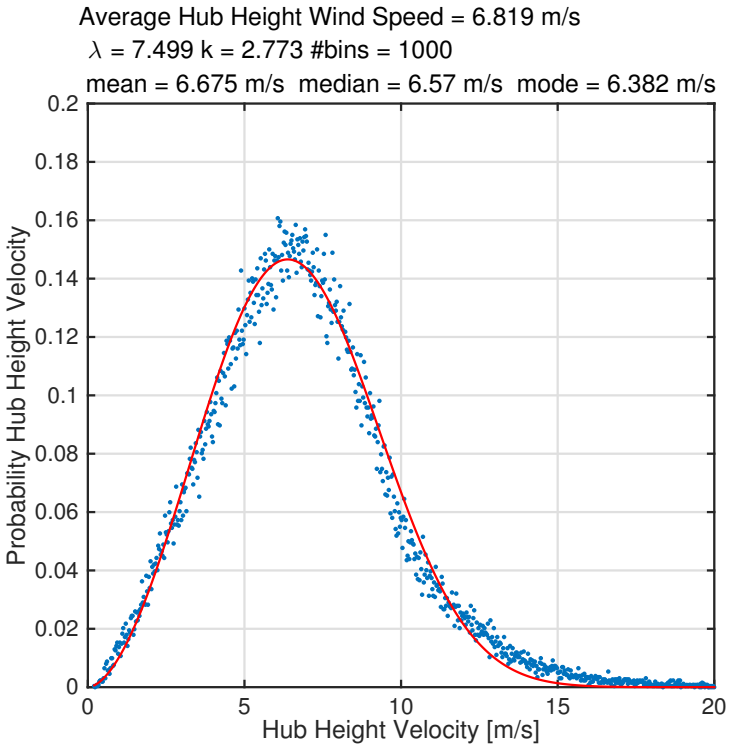

Figure 3.2. Probability of wind speed at hub height.

$$Pr(U_\infty) = \frac{k}{\lambda}\left(\frac{U_\infty}{\lambda}\right)^{k-1} e^{-(U_\infty/\lambda)^k}. \tag{3.1}$$

The wind direction was calculated at hub height as seen in Figure 3.3, with the average wind coming from the South with an average heading of 176°. The probability of a wind from the south, plus or minus 10° is 14.6%, ±20° is 26.3%, ±30° is 34.6%, and ±40° is 42.2%. The tower wake directional sector is shown in this plot, shaded in red.

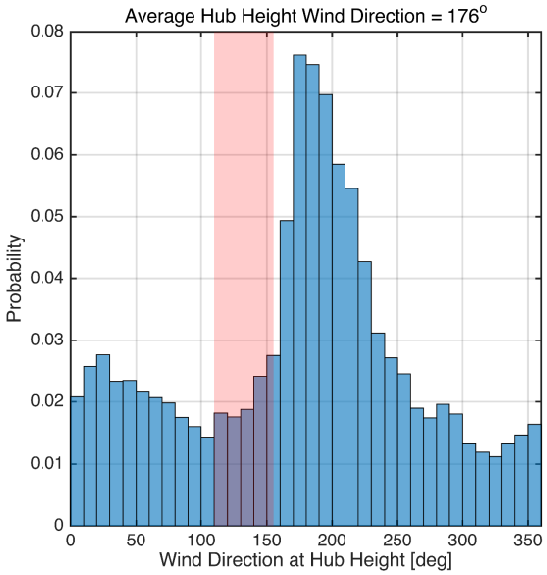

Figure 3.3. Probability of wind direction at hub height, [3,20] m/s.

The probability distributions and mean values , shown as $<>$, of turbulence intensity, density, temperature, relative humidity, pressure, and power law shear exponent are summarized in Figure 3.4. The average turbulence intensity is 12.9%, with average power law exponent $\alpha = 0.21$. The turbulence and shear constant histogram have the 110°–155° wind sector removed due to the tower wake. The SWiFT site is located 1021 m above sea level and the average air density is 1.08 kg/m^3. What is interesting is the amount of spread in the density over the data range which directly scales the energy in the wind and varies approximately ±10%. This will need to be taken into consideration for future experimental campaigns and model validation efforts.

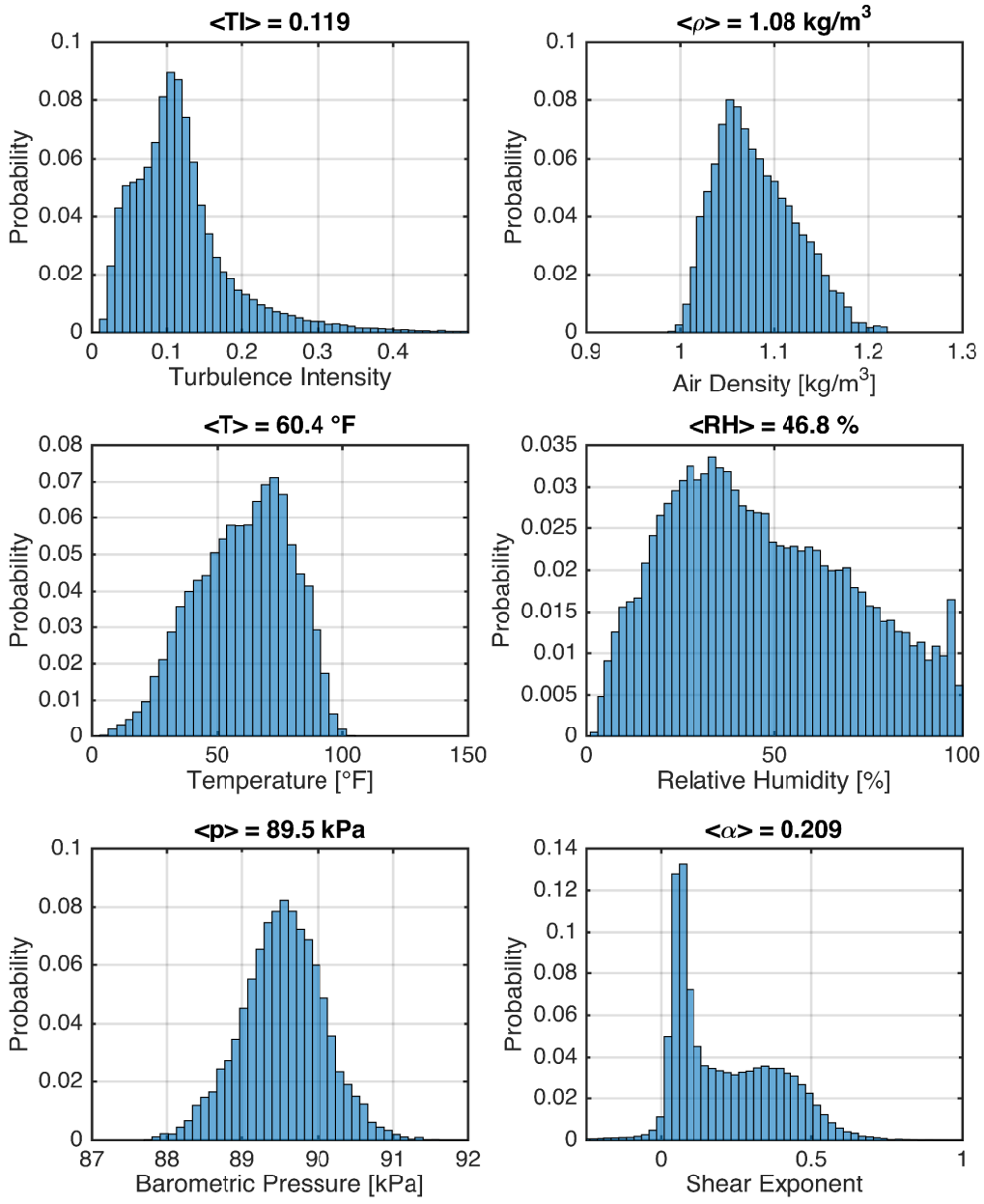

Figure 3.4. Probability and mean of various quantities interpolated at hub height, [3,20] m/s.

Table 3.1. Annual Average Atmospheric Quanitities.

Atmospheric Variable	All Wind Speeds	Wind Turbine Range
Wind Speed (m/s)	6.8	–
Wind Direction	176°	
Turbulence Intensity	12.9%	11.9%
Velocity Profile Shear Exponent	0.208	0.209
Air Density (kg/m^3)	1.08	

The frequency of the atmospheric stability classes from the full data set is shown in Figure 3.5. Based on the definition of "near-neutral", stable and unstable classes are then defined. There is some variation dependent upon this definition but it is likely conservative to say that neutral cases occur less than about 10% of the time. From this figure it is observed that the stable class for atmospheric stability is most frequent at the site at around 50% frequency.

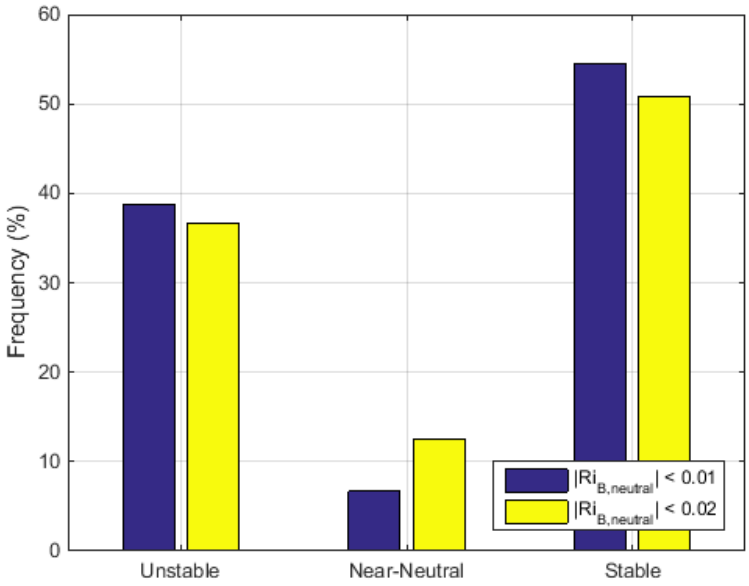

Figure 3.5. Frequency of Stability Conditions at the SWiFT Site, [3,20] m/s.

A wind rose with frequency of wind speed ranges per directional bins is plotted in Figure 3.6. This graph reveals the most frequent South and South-West wind directions as discussed earlier, but also shows where the high wind conditions are most frequent. The highest wind speed conditions seem to occur most frequently from the South and South-West, and from the North. The directional sector from 110°–155° is within the most infrequent wind direction section, and additionally contains mostly only very low wind resource.

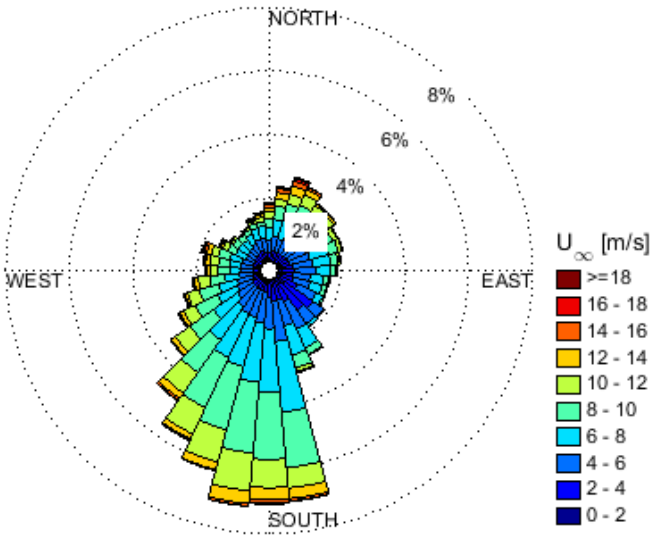

Figure 3.6. Cumulative Wind Rose for the SWiFT Site.

3.1.1 IEC Classification

The SWiFT site IEC classification is determined to be a class III-C. Wind turbine designs are governed by standards which place requirements on the machine that differ based on the site classification. These specific requirements and the classification can be found in the standard *IEC 61400-1 Ed.3: Wind turbines - Part 1: Design Requirements* [3]. The IEC design standard is in reference to the turbine site's particular conditions with the site being designated by a numeric class (I-III) based on average wind speed at hub height, and a letter (A-C) based on the average turbulence intensity at 15 m/s. This classification is listed in Table 3.2.

Table 3.2. IEC Site Classification [3].

Wind Turbine Class	I	II	III
V_{Avg} (m/s)	10	8.5	7.5
A	$I_{ref@15\ m/s}$: 0.16		
B	$I_{ref@15\ m/s}$: 0.14		
C	$I_{ref@15\ m/s}$: 0.12		

The analysis of the atmospheric conditions at the SWiFT site reveal a hub height average wind speed of 6.8 m/s, making it a class III. The average turbulence intensity (TI) is shown in Figure 3.7, compared with the IEC turbulence classification TI curves. The grey background dots are each 10 min averages from the data with the orange line showing the bin-average of this data. At 15 m/s

the orange line is below the C-class of turbulence. The IEC normal turbulence model assumes the form $TI = I_{ref}(\frac{3}{4} + \frac{5.6}{U_\infty})$. A curve of this form was fit, with $I_{ref} = 0.11$ which reduced the squared error at 15 m/s as called for by the standard. This defines the turbulence class as Class C ($I_{ref} = 0.12$).

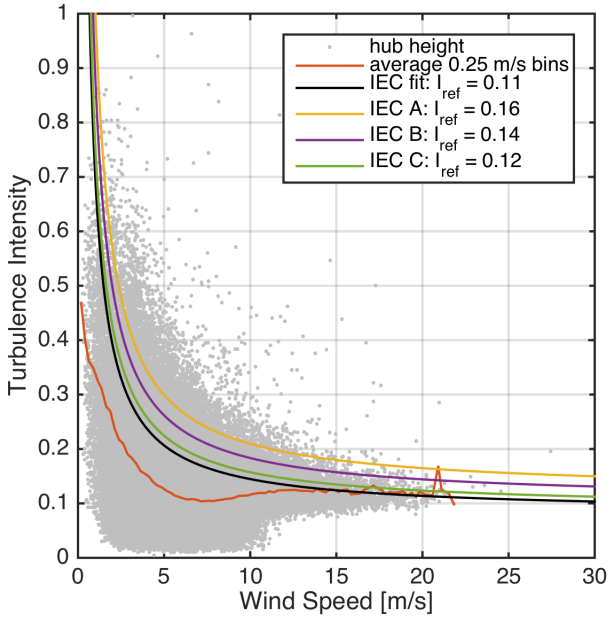

Figure 3.7. IEC normal turbulence model.

3.2 Hourly Atmospheric Trends

This section focuses on the average day. Every 10 min average data point has been grouped into bins equal to the hour of the day in which that 10 minutes occurred. Lubbock observes daylight savings time, however for clarity, the following figures use UTC-06:00 (Central Standard Time) for all data. Figures 3.8 and 3.9 show how mean wind speed and turbulence intensity vary with height above ground level (AGL) throughout the day. At the higher tower stations the mean wind speed increases during the night whereas at lower tower stations the average wind speed increases during the day, due to the increased daytime turbulence and mixing. There is less shear at most tower heights and greater turbulence intensity from 12:00–16:00 due to turbulent mixing from ground heating. Accordingly, there is less turbulence at night from 20:00–07:00 on the average day as seen in Figure 3.10.

Atmospheric stability describes how much buoyancy is contributing to turbulent mixing within the atmosphere. Virtual potential temperature change in height, $\Delta\theta_v$, describes this thermal gradient. The Bulk Richardson Number, Ri_B, is proportional to virtual potential temperature change. Positive values of the Bulk Richardson number are for stable conditions where the potential temperature increases with height. Negative values describe conditions where buoyancy creates vertical mixing, leading to a more uniform mean boundary layer profile. All 10 min data points were

binned by the hour of occurrence a definition of stable, neutral, and unstable conditions based on the difference in virtual potential temperature 0.9 m and 2.4 m AGL, shown in Figure 3.11. Hours of the day when these stability conditions most frequently occur is observed. Stable conditions occur most at night, and unstable conditions during late morning and afternoon with neutral transitions in between, as summarized in Table 3.3. The range of typical shear exponents is as low as 0.05 at 11:00, and as high as 0.34 at 06:00 as seen in Figure 3.12.

Table 3.3. Stability Class Average Transition Time of Day.

Stability Class	Stable	Neutral Transition	Unstable	Neutral Transition
Time of Day	20:00–08:00	08:00–10:00	10:00–18:00	18:00–20:00

3.2.1 Average Day Trends

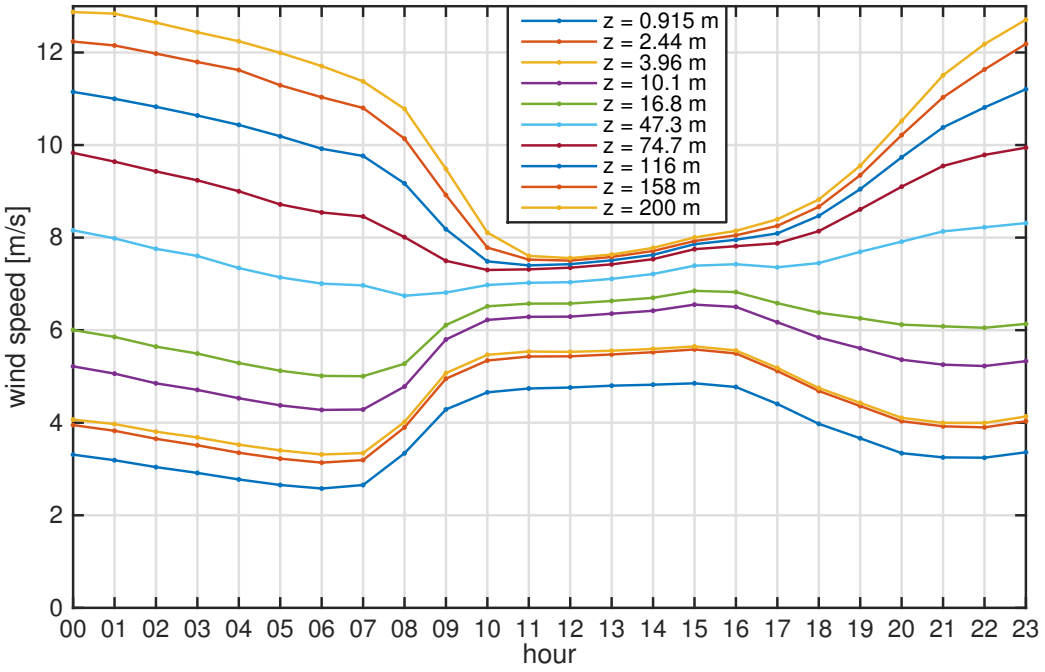

Figure 3.8. Average day wind speed.

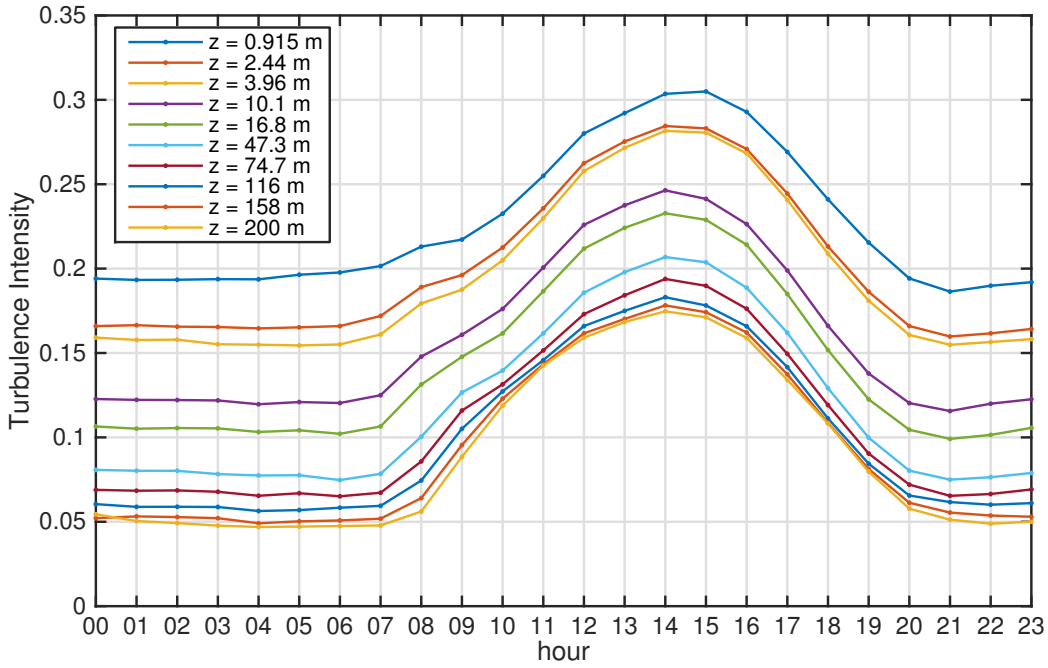

Figure 3.9. Average day turbulence intensity, [3,20] m/s.

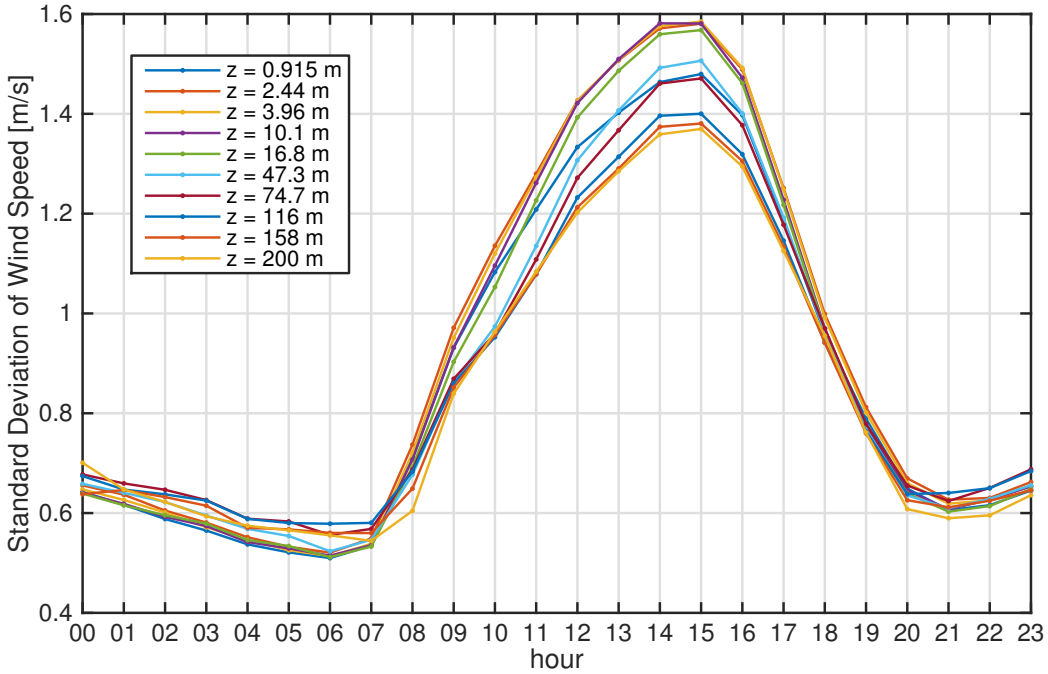

Figure 3.10. Average day wind speed standard deviation, [3,20] m/s.

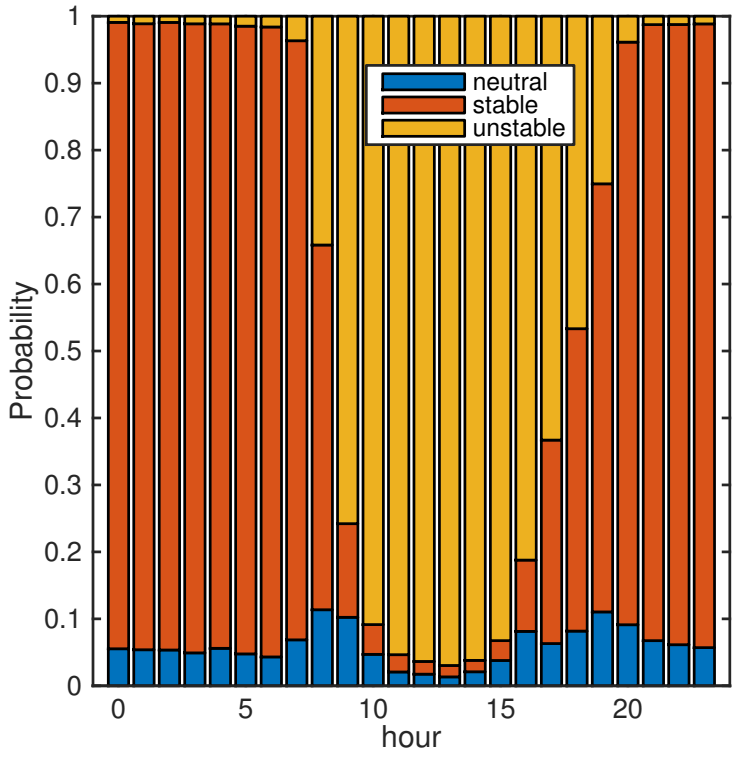

Figure 3.11. Average day stability, [3,20] m/s. Stable 20:00–07:00, Unstable 09:00–17:00, Neutral 08:00–09:00 and 18:00–19:00.

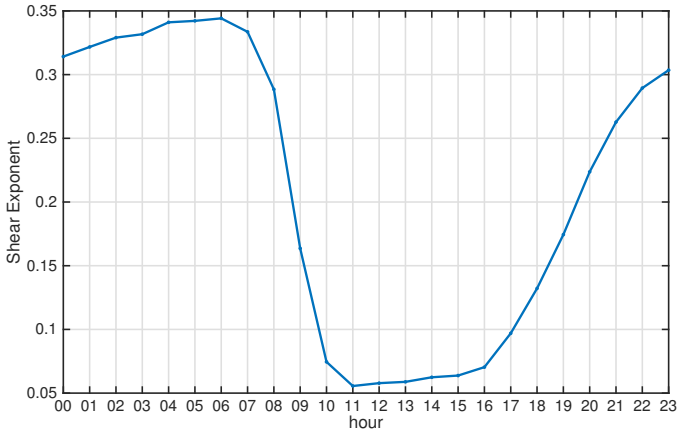

Figure 3.12. Average day power law exponent, [3,20] m/s.

3.2.2 Average Day Model Inputs

The boundary layer profiles of mean wind speed, turbulence intensity, virtual potential temperature, and veer for the hours of the day summarized in Table 3.3 are presented in Figure 3.13. These hours are approximations of average stability classes and transitions. These can be used as parameters or boundary conditions for various wind farm simulations that are representative of the most common stable, neutral, and unstable conditions at SWiFT. The mean conditions for all time do not describe well neutral conditions due to this transition's dependency on time of year, but the stable and convective conditions are considered to be representative in the average. As expected, unstable conditions lead to a full boundary layer profile with higher wind speeds close to the ground and significantly higher turbulence intensity at all heights. The virtual potential temperature profiles show a strongly stable condition but the average is a weakly convective boundary layer. The temperature decreases with altitude, especially over the first 20 m in unstable conditions. In neutral conditions based on the bulk Richardson number, the temperature profile is more constant with altitude than is seen in this averaged analysis due to averaging additional stability classes with the neutral case.

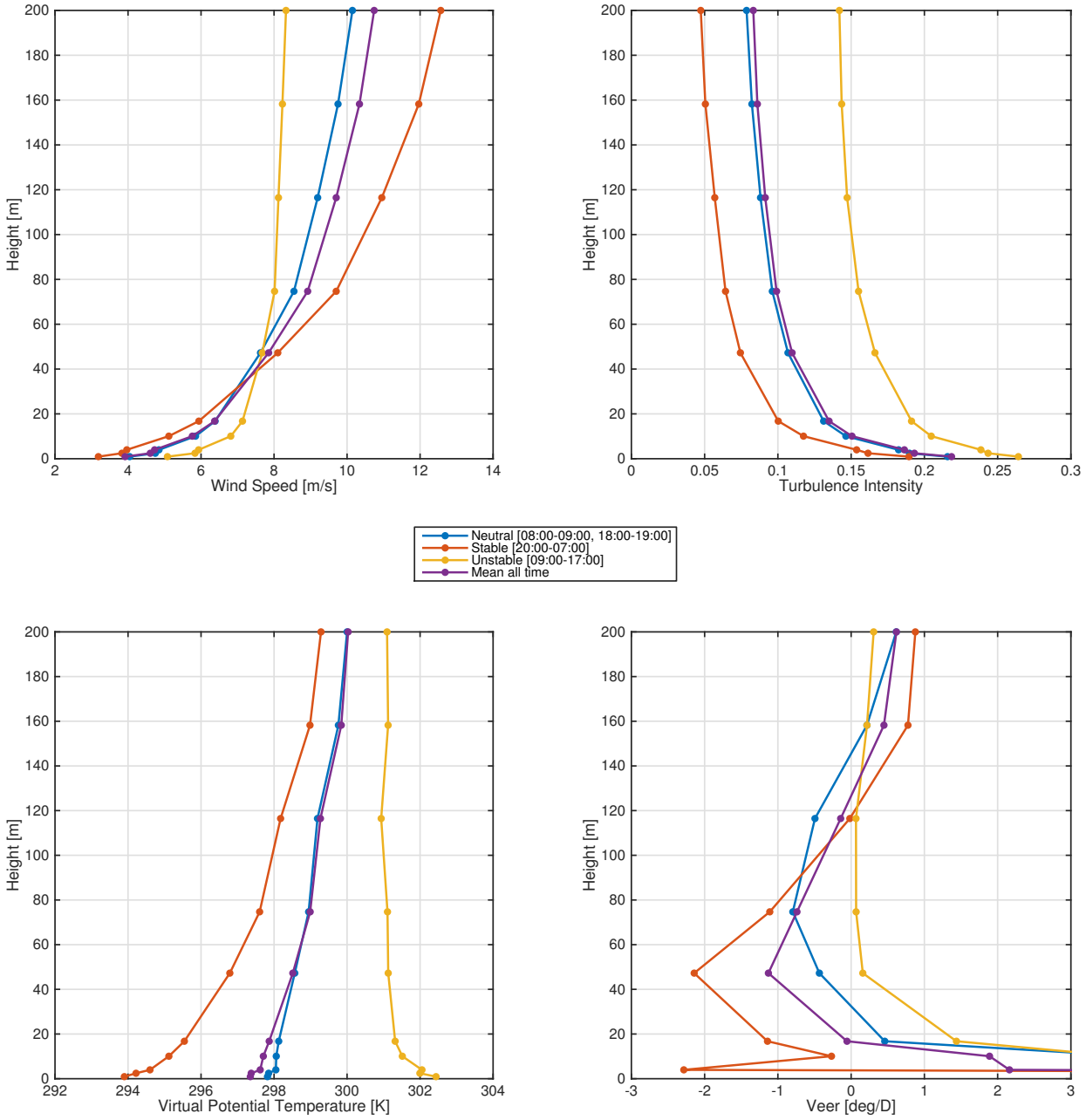

Figure 3.13. Representative boundary layer profiles for the Scaled Wind Farm Technologies site, [3,20] m/s.

3.3 Monthly Atmospheric Trends

The seasons also have a significant effect on atmospheric conditions. All 10 min data points within the same month were grouped together at each of the meteorological tower heights. Figure 3.14 shows how the wind speed changes for each month of a typical year. July–September at all tower heights showed consistently lower average wind speeds, while March, June, and April showed the highest average wind speeds. Unlike hour of the day, the month has less effect on shear, as evidenced by the differences between wind speeds at all tower heights remaining constant for each month. By fitting the boundary layer profile with the power law profile the power law exponent, α, was found describing heights between 17 m and 158 m. These heights were used because they would span rotor disc heights from subscale to full-scale. Figure 3.18 shows that the fullest boundary layer profile is in June with $\alpha = 0.17$, and the most laminar profile is in November, $\alpha = 0.25$.

Seasonal changes also affect wind direction and atmospheric turbulence. Figure 3.15 shows that for any month the average wind direction is predominantly from the south. September has the most easterly wind, SSE around 158°, and December the most westerly, nearly SSW. February and October are most likely to have winds directly from the south. Turbulence intensity can be seen in Figure 3.16. The most turbulent months at all tower heights occurred from June–August. The lowest turbulence intensity was in December and January.

Figures 3.19–3.22 show how air density, temperature, relative humidity, and barometric pressure change throughout the typical year as a function of height above ground level. August has the second lowest density and lowest wind speed, and therefore will likely be the worst for energy production in a typical year. April has an average density and the highest average wind speed, therefore April likely has the most wind energy available. Figure 3.23 shows that every month has approximately the same number of neutral atmospheric stability cases. The summer months more commonly have unstable conditions, and the winter more commonly has stable conditions.

3.3.1 Average Year Trends

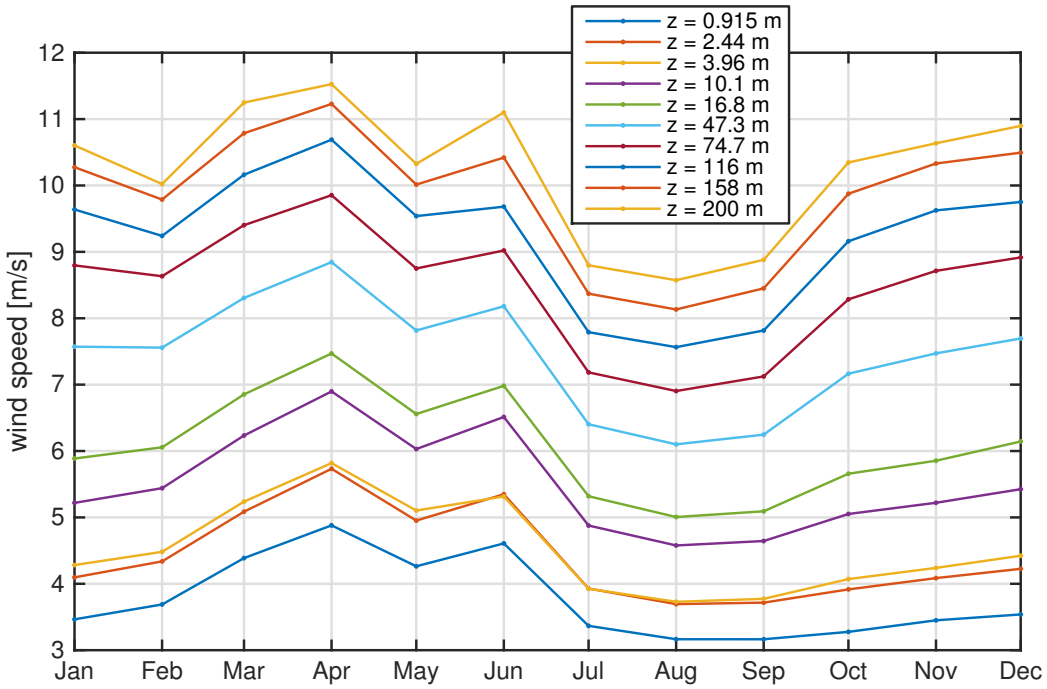

Figure 3.14. Average year wind speed.

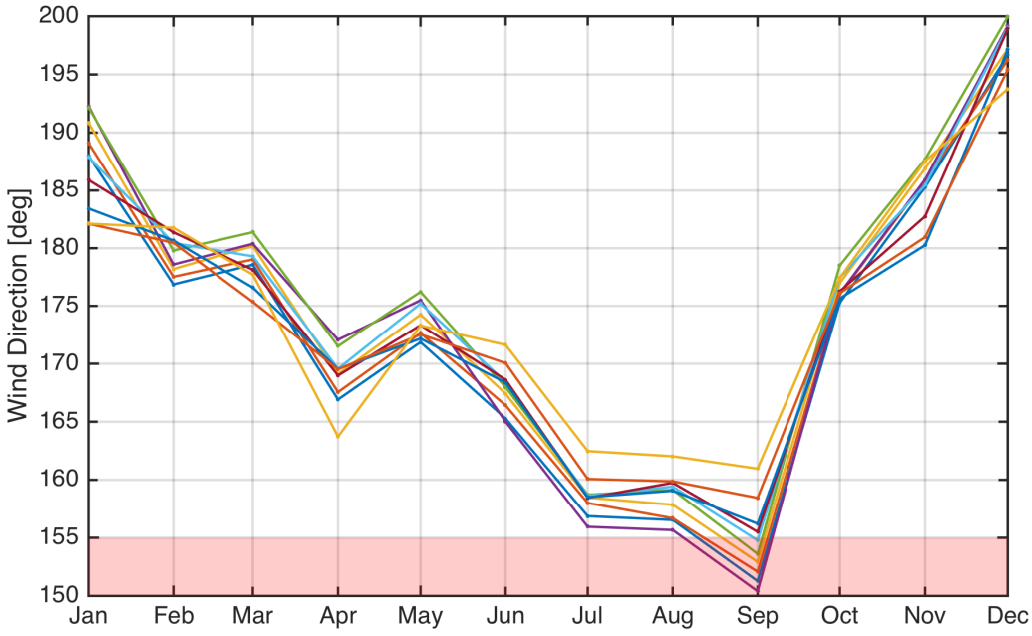

Figure 3.15. Average year wind direction, [3,20] m/s.

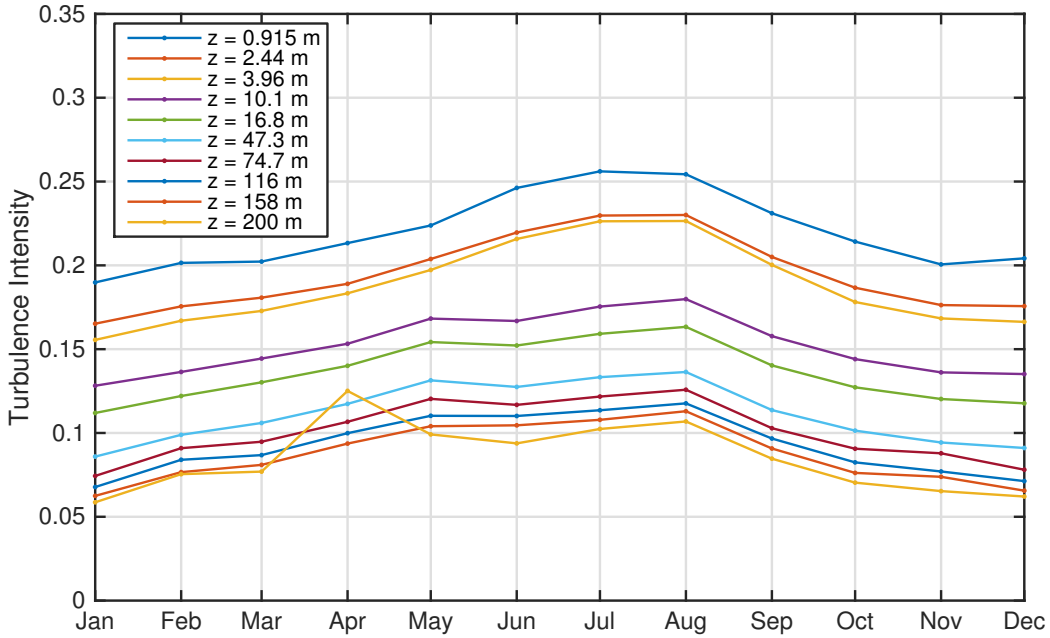

Figure 3.16. Average year turbulence intensity, [3,20] m/s.

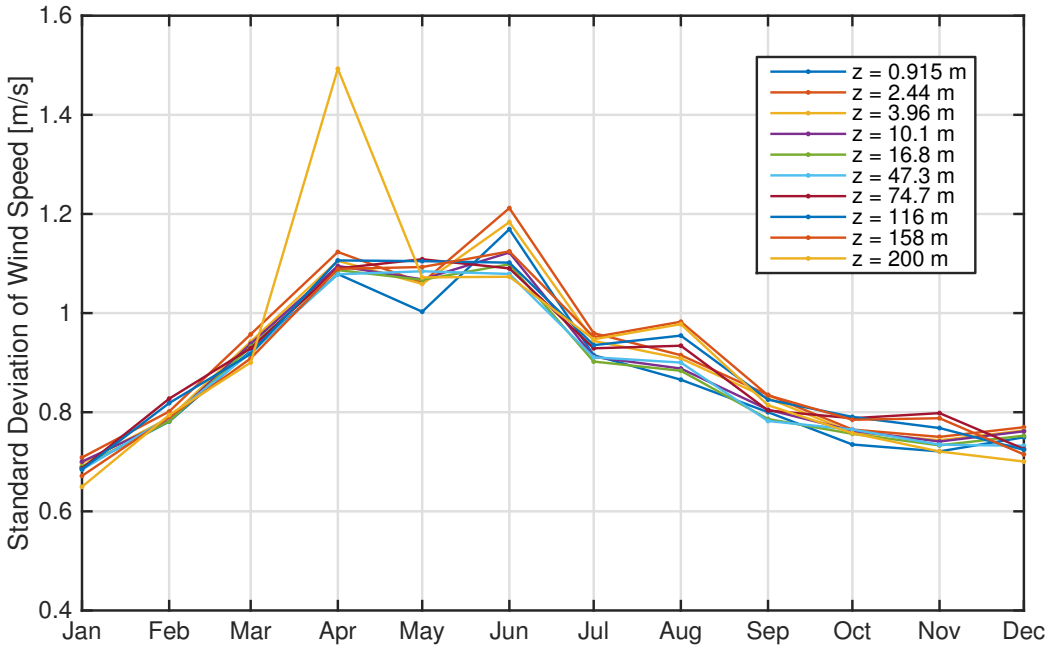

Figure 3.17. Average year wind speed standard deviation, [3,20] m/s.

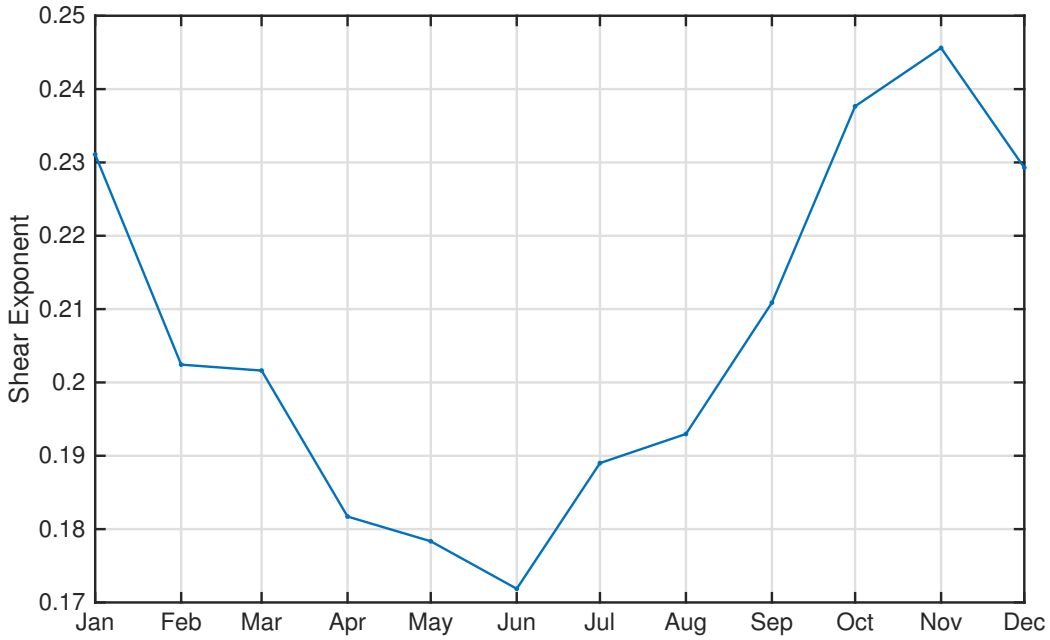

Figure 3.18. Average year power law exponent, [3,20] m/s.

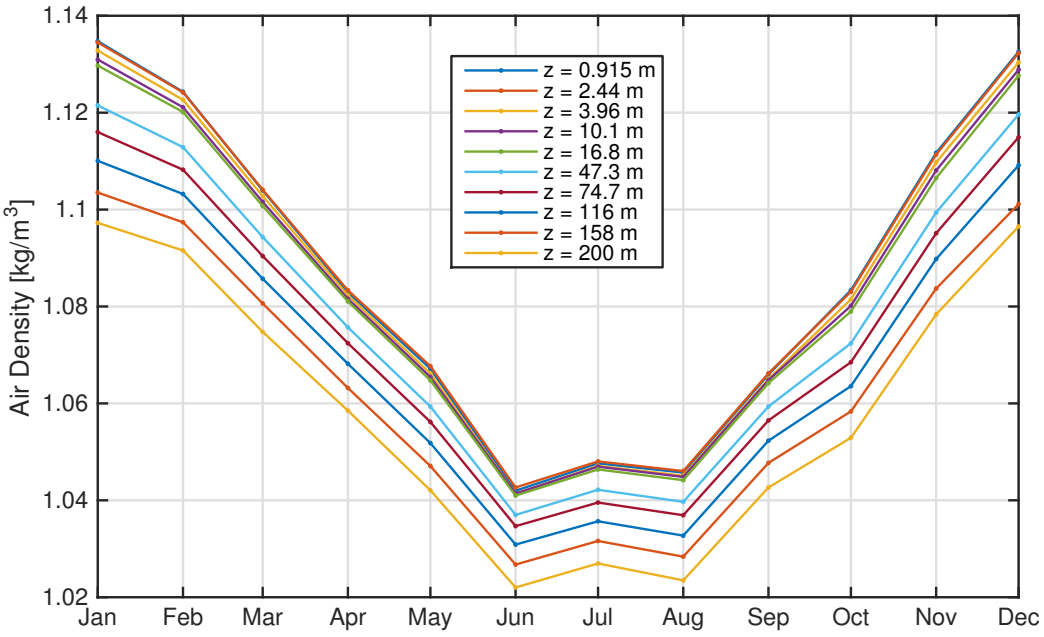

Figure 3.19. Average year density.

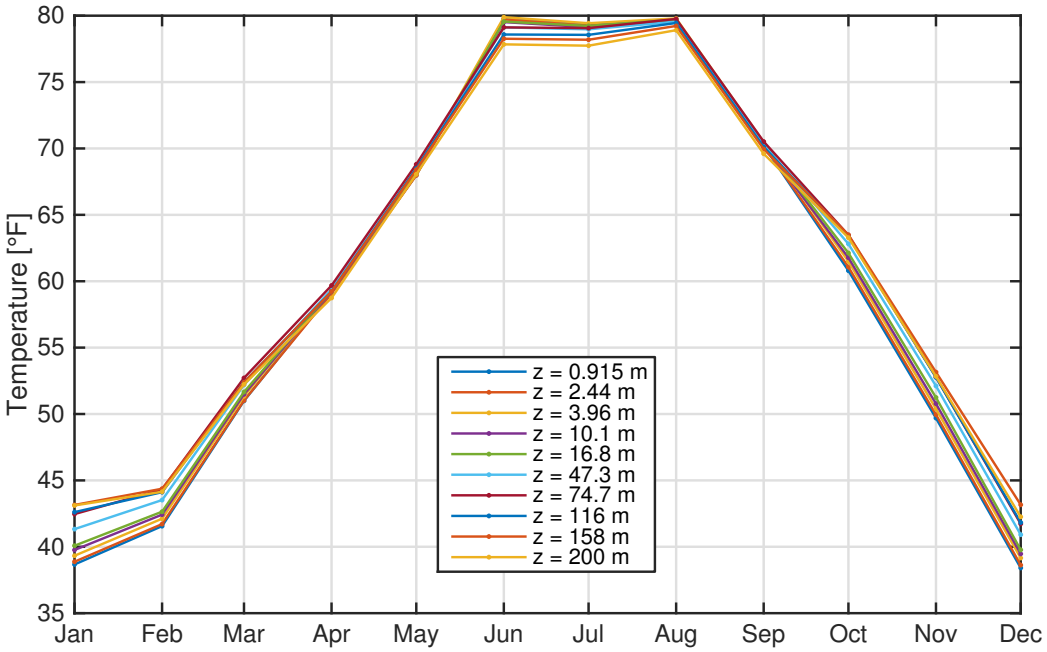

Figure 3.20. Average year temperature.

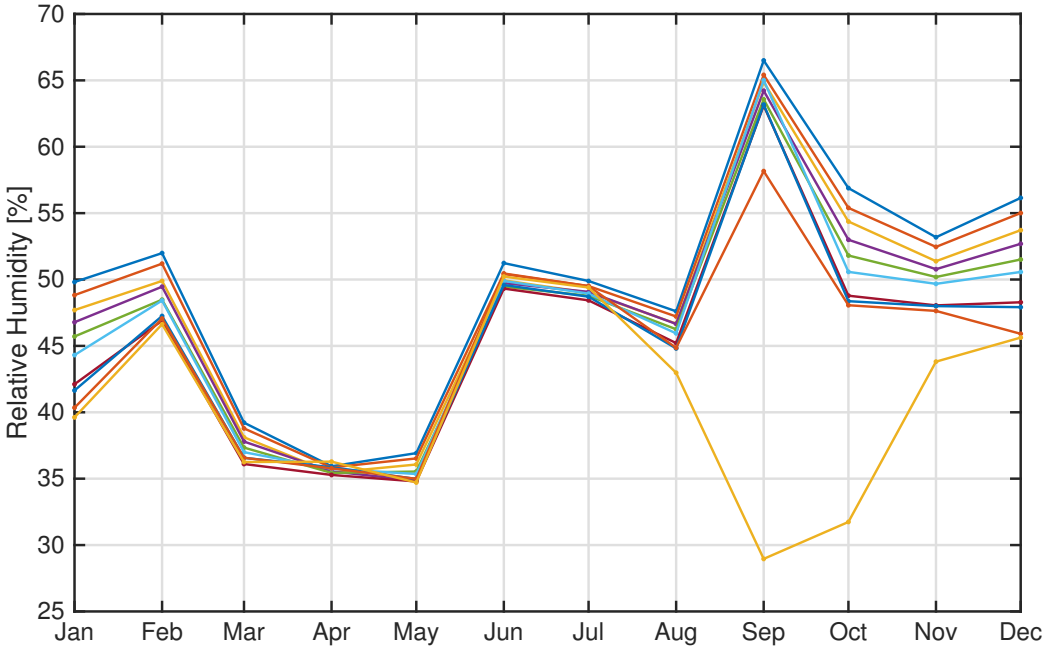

Figure 3.21. Average year relative humidity.

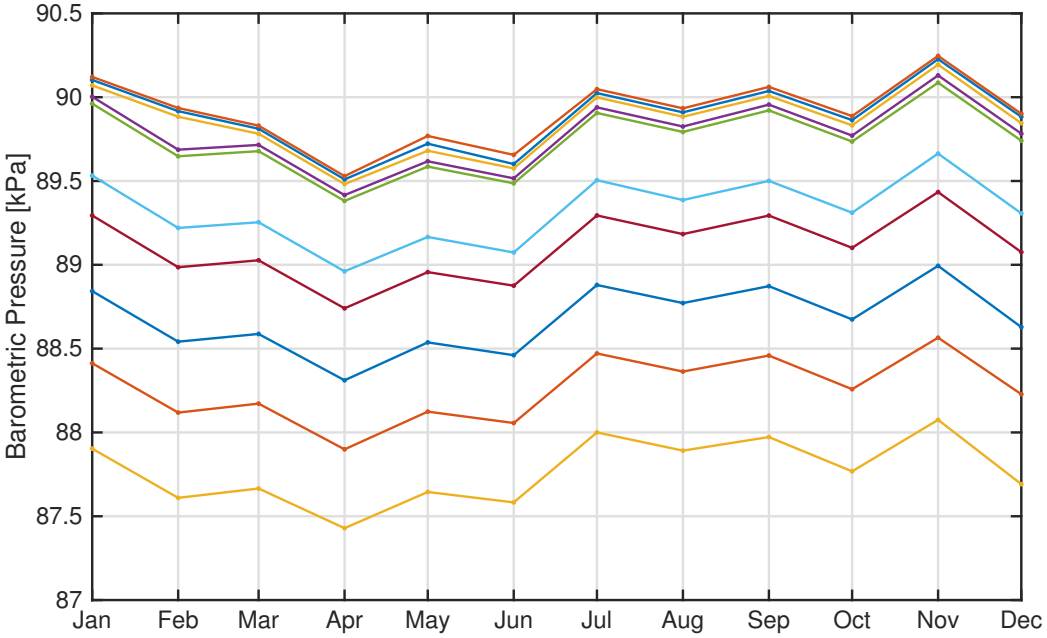

Figure 3.22. Average year barometric pressure.

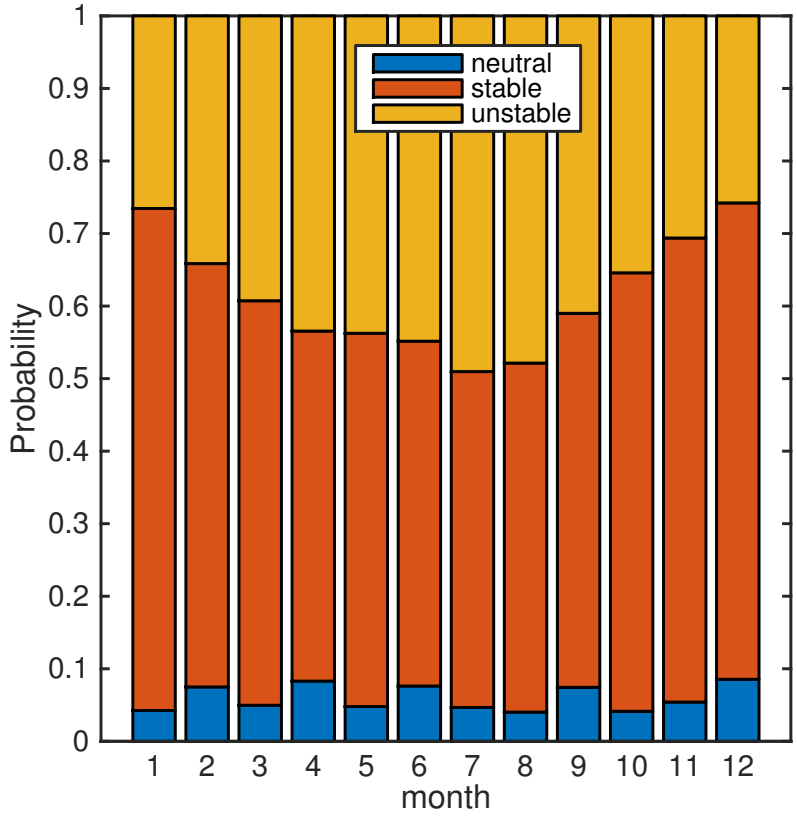

Figure 3.23. Probability of stability in the average year, [3,20] m/s.

3.3.2 Correlation of Wind Speed and Turbulence Intensity

The wind speed and turbulence dependency is important for planning an experiment because not all combinations of values are likely to occur at the same time. The joint probability was found for wind speeds in groups of 5 m/s and turbulence intensity groups of 0.05. The probability for each pair is a joint probability which is calculated by the number of occurrences of intersection of the ith and jth conditions divided by the total number of data points, N.

$$Pr(U_{\infty i} \cap TI_j) = \frac{N(U_{\infty i} \cap TI_j)}{N} \tag{3.2}$$

Table 3.4 tabulates these results such that the values in the table are the probabilities as a percentage in which the various conditions occur simultaneously. For example a wind speed of 5–10 m/s and a turbulence intensity of 5–10% occur simultaneously 22.3% of the time. The sum of all the joint probabilities is 100%. The most common pairs of occurrences are 5–10 m/s wind speeds with 5–10% turbulence intensity. The next most common pair is 5–10 m/s wind with 10–15% turbulence intensity. And the third most common pair is 5–10 m/s wind with 0–5% TI. These three cases all have the same range of wind speeds and account for over 52% of all data.

Table 3.4. Probability as a percent (joint distribution) of wind speed and turbulence intensity combinations at hub height.

	0–0.05	0.05–0.1	0.1–0.15	0.15–0.2	0.2–0.25	0.25–0.3
0–5	3.3	6.4	5.6	3.7	2.6	2.1
5–10	8.8	22.3	21.2	7.2	2.9	1.1
10–15	0.1	2.3	8.0	1.2	0.2	0.0
15–20	0.0	0.1	0.8	0.1	0.0	0.0

3.3.3 Monthly Wind Rose and Speed Distribution

The wind rose shows how common different wind directions are and what range of wind speeds are present in these directions. Figures 3.24–3.26 show the wind rose for every month. June has the most wind directly from the South. July, August, and September also have high probabilities of southerly winds. It is worth noting that the defined tower wake sector is 110°–155°, which serves to artificially reduce the wind speed in this region.

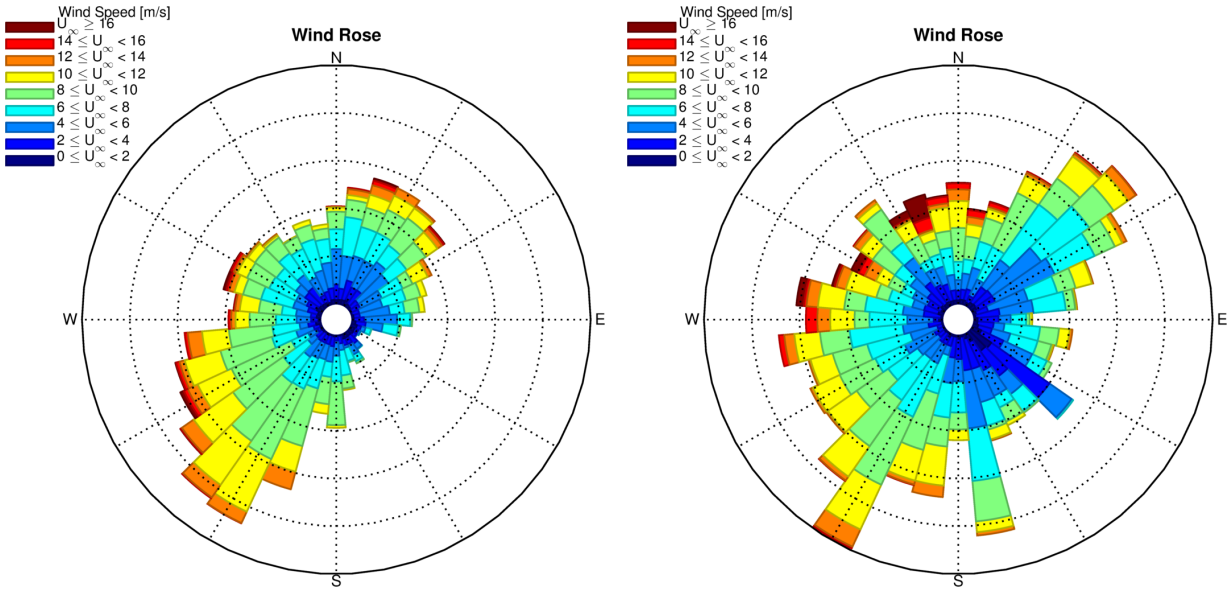

(a) January **(b)** February

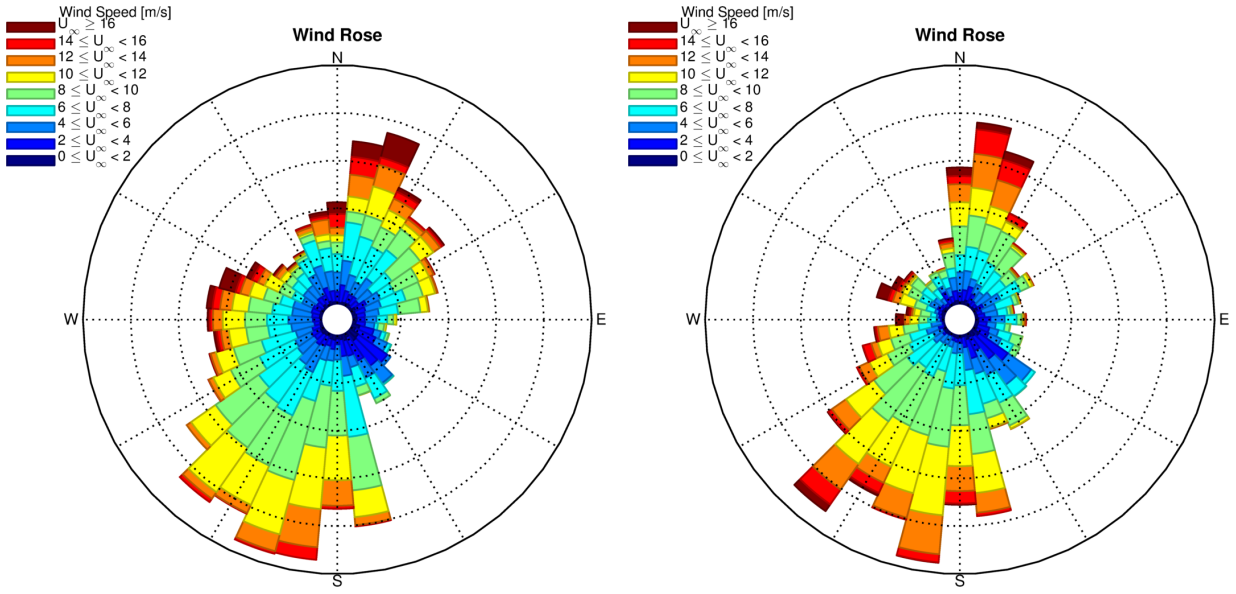

(c) March **(d)** April

Figure 3.24. Wind rose with wind speed intensity, January–April.

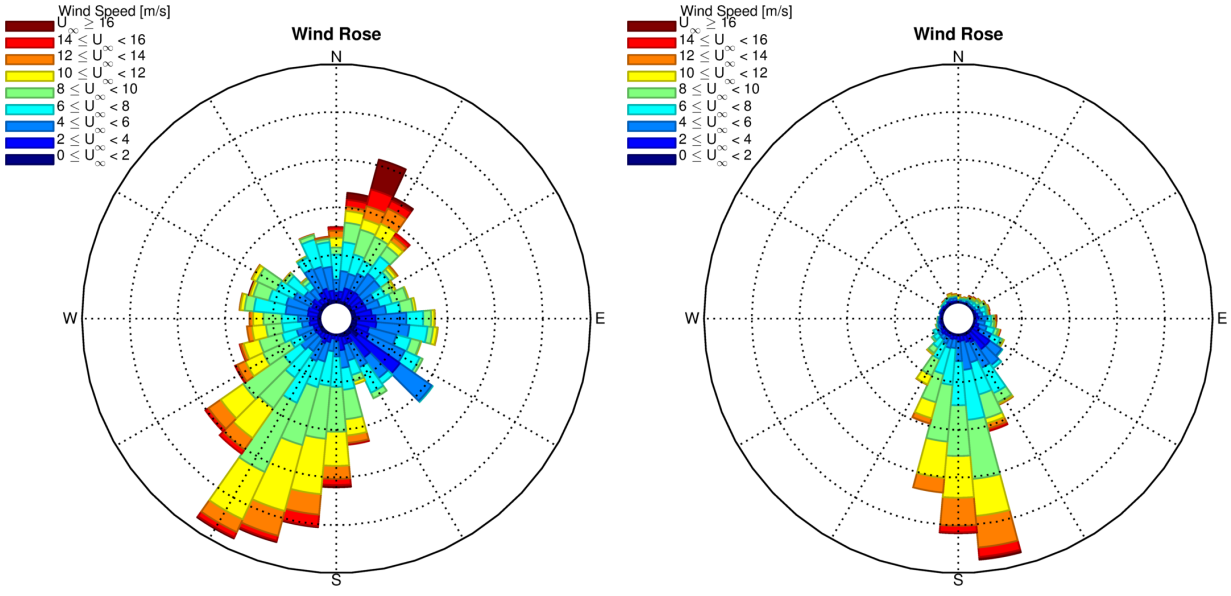

(a) May **(b)** June

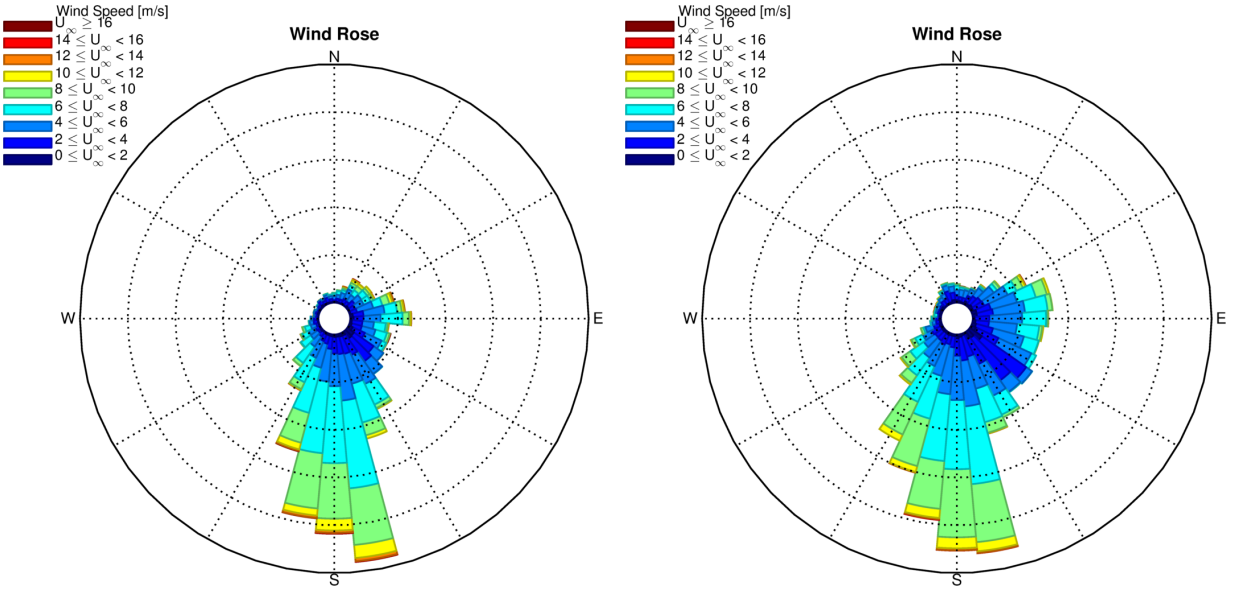

(c) July **(d)** August

Figure 3.25. Wind rose with wind speed intensity, May–August.

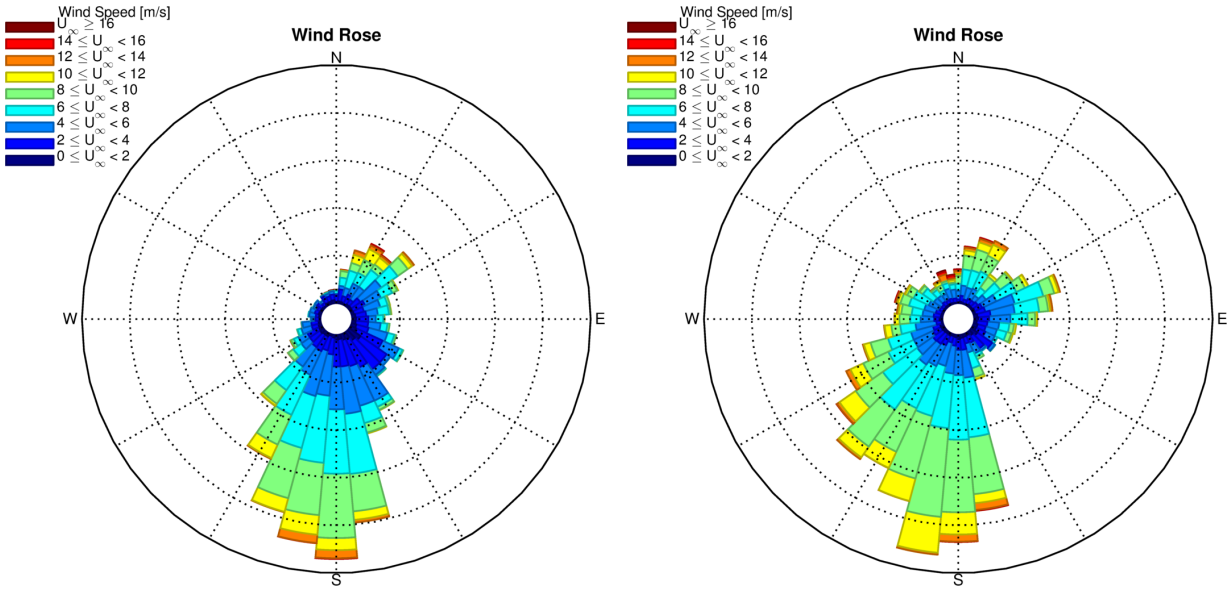

(a) September **(b)** October

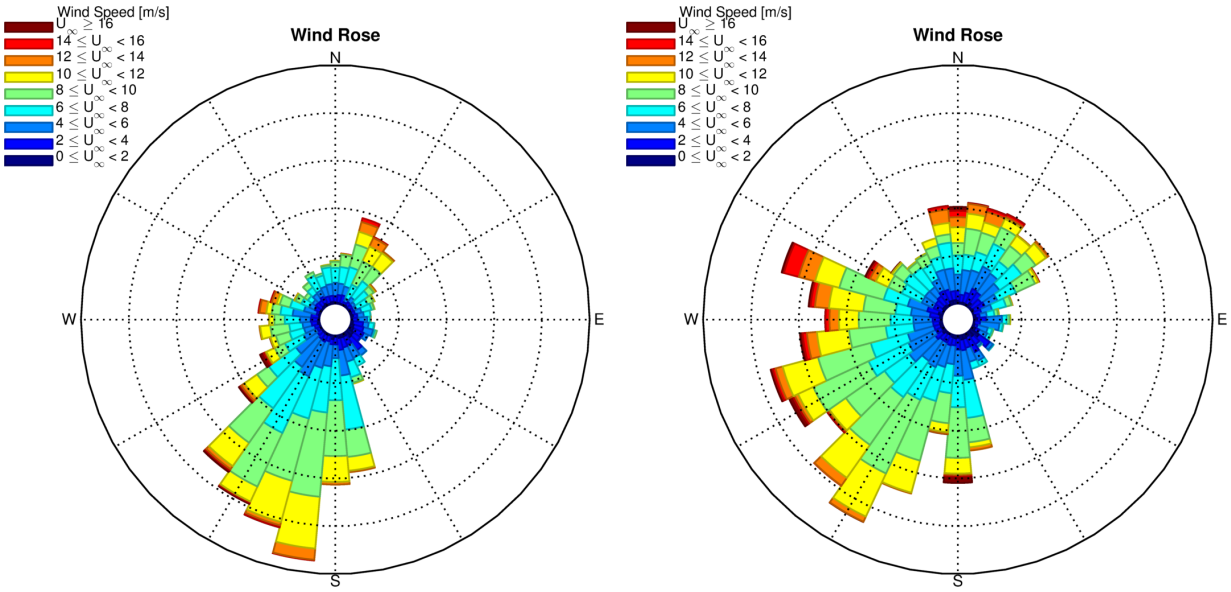

(c) November **(d)** December

Figure 3.26. Wind rose with wind speed intensity, September–December.

3.4 Correlation of Atmospheric Quantities for Single Turbine Tests

The correlation of select atmospheric quantities is shown in this section. This section does not additionally add the requirement for turbine-turbine interaction which would serve to limit the wind direction sectors. That additional condition will be discussed in the next section.

3.4.1 Velocity Shear and Veer Trends

Turbulence intensity at hub height is likely to cause greater vertical mixing and hence a fuller, more turbulent velocity profile. This corresponds to a lower power law profile exponent, α. This can be seen clearly in Figure 3.27. The trend line averages all data into turbulence bins 0.01 in width. The maximum average shear profile exponent is $\alpha = 0.36$ at a turbulence intensity of TI = 0.065.

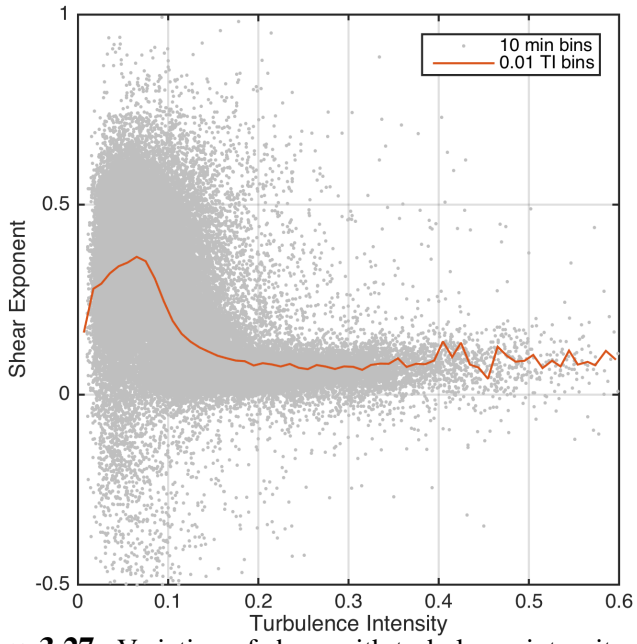

Figure 3.27. Variation of shear with turbulence intensity at hub height, [3,20] m/s.

Veer is the change in wind direction per unit distance from the ground, that is $\frac{d\theta}{dz}$. Positive veer corresponds to a wind direction moving clockwise on the compass rose with increasing height, and negative values counter-clockwise. The veer of interest is that across the SWiFT turbine rotor disk, using the two adjacent tower measurement stations at 16.8 and 47.3 m (55 and 155 ft), and the units of veer in this analysis are degrees per rotor diameter. Figure 3.28 shows a clockwise veer is more common that counter-clockwise veer. And at 7 m/s, the average wind direction is 2° higher clockwise at the rotor top than at the rotor bottom. Figure 3.29 shows that turbulence reduces the amount of veer and the greatest amount of average veer is when the turbulence intensity is at 5%.

Figure 3.30 shows that the shear profile constant is semi-correlated with veer where veer most commonly occurs with large shear, as is expected for overnight stable atmospheric conditions.

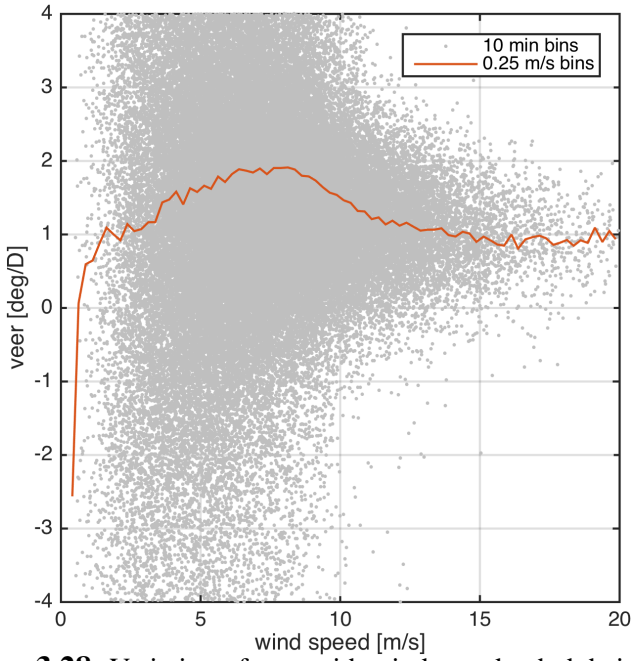

Figure 3.28. Variation of veer with wind speed at hub height.

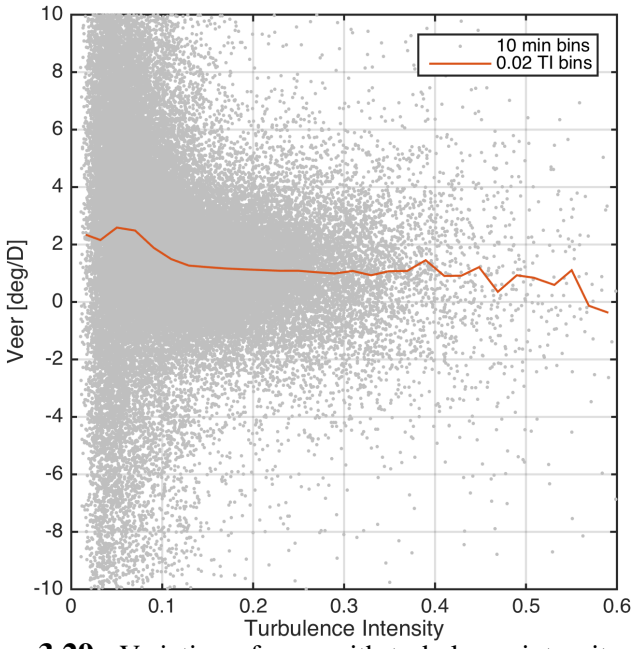

Figure 3.29. Variation of veer with turbulence intensity at hub height, [3,20] m/s.

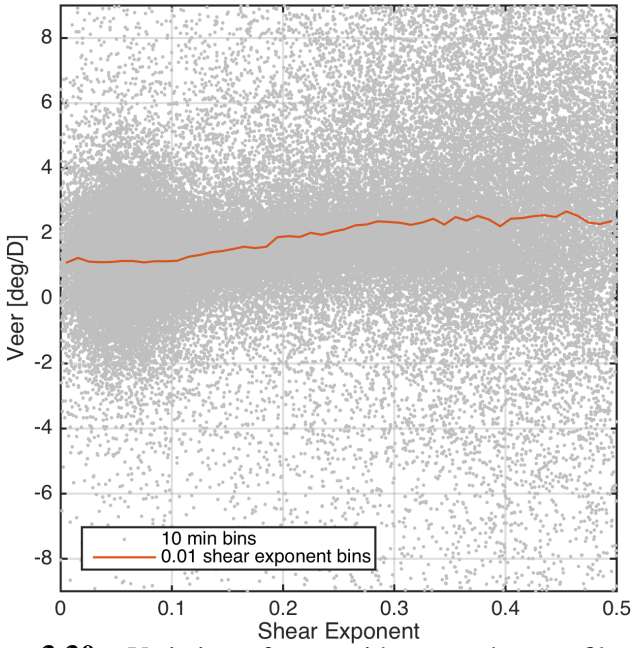

Figure 3.30. Variation of veer with power law profile at hub height, [3,20] m/s.

3.4.2 Atmospheric Stability Trends

The following bar charts show how mean wind speed, turbulence intensity and the shear exponent vary with atmospheric stability. The values are stacked, not overlaid, and the total probabilities sum to 1. Figure 3.31 demonstrates neutral stability leads to the highest wind speeds at hub height with a median and mode higher than for stable and unstable conditions. Figure 3.32 shows how the distribution of turbulence intensity changes with stability conditions. For neutral stability the most common TI is 13%. At lower TI stable conditions are most likely and above 13% unstable conditions are most likely. Figure 3.33 shows that stable and unstable conditions are most common with southerly winds, while neutral conditions occur most from northerly winds. Figure 3.34 shows how the most common shear constant varies with stability conditions. Unstable atmospheric conditions have the lowest α values typical of a turbulent boundary layer, with 0.05 the most common. During neutral conditions a shear constant of 0.125 is the average, and stable conditions show the largest shear constants. Finally, Figure 3.35 demonstrates that larger values of veer occur most for stable conditions as would be expected.

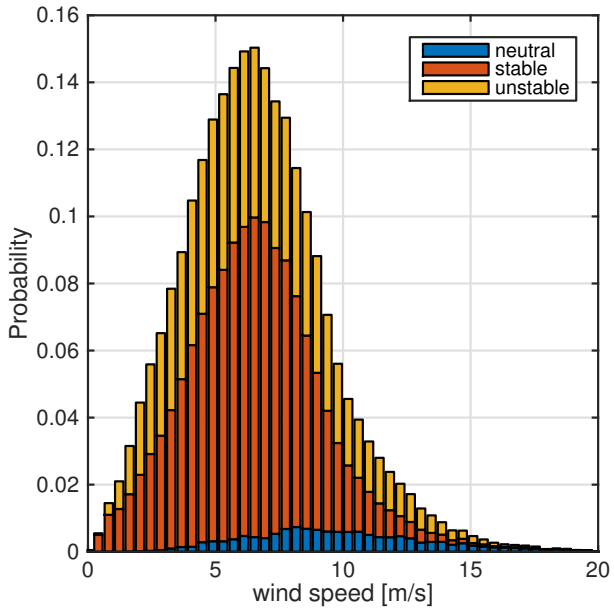

Figure 3.31. Probability of hub height wind speeds for various stabilities.

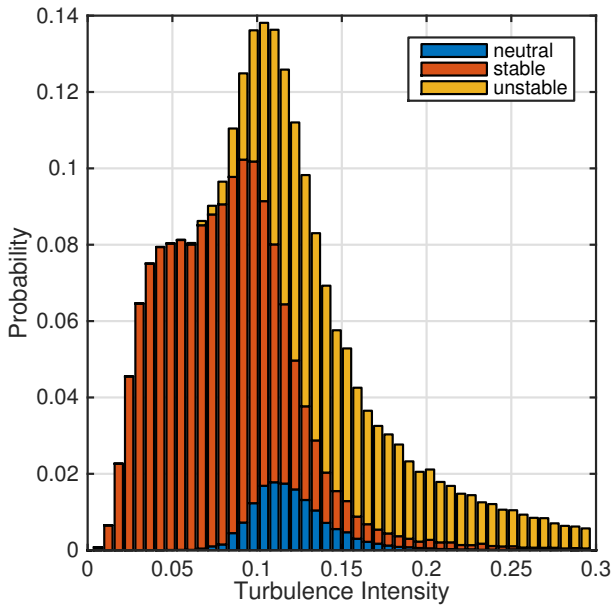

Figure 3.32. Probability of turbulence levels for various stabilities, [3,20] m/s.

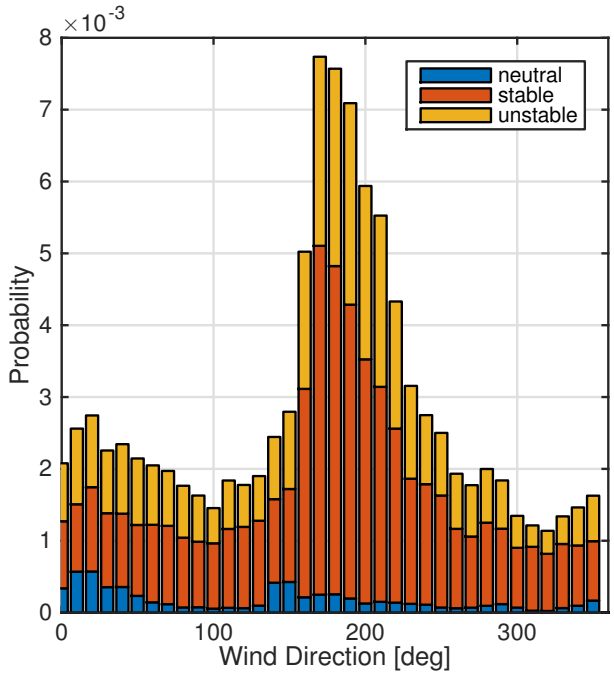

Figure 3.33. Probability of wind directions for various stabilities, [3,20] m/s.

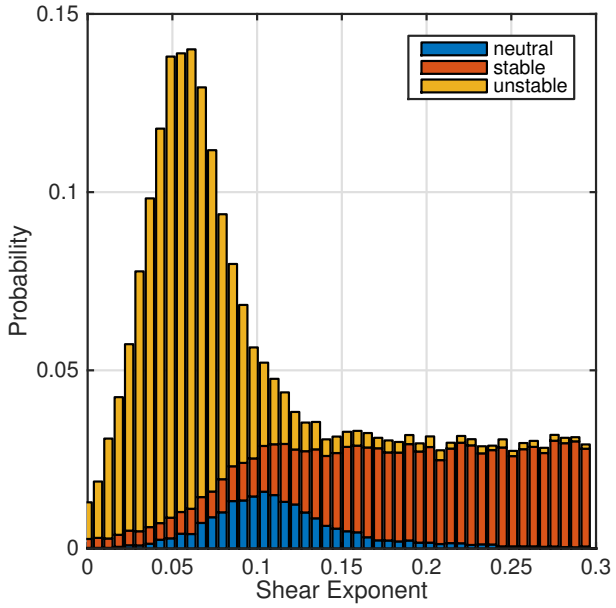

Figure 3.34. Probability of shear profiles for various stabilities, [3,20] m/s.

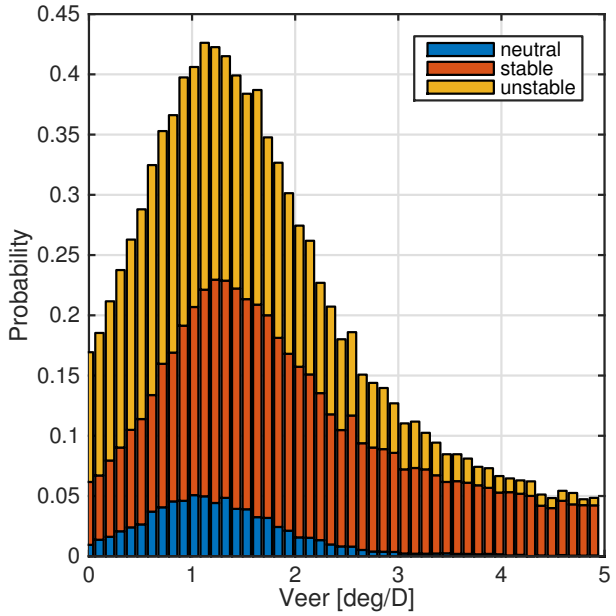

Figure 3.35. Probability of veer for various stabilities, [3,20] m/s.

3.5 Correlation of Atmospheric Quantities for Turbine-Turbine Tests

With turbine-turbine tests, the wind direction is a criterion for probability because this quantity determines the waked condition and interaction of the array. As a reminder, the turbine-turbine interaction with a 5 diameter is exactly aligned for a 180°/0° incoming wind, and the turbine-turbine interactions with 6 diameter and 3 diameter spacing's are exactly aligned at 210°/30° and 266°/86°. The joint probability was found for wind direction in groups of 30° sectors for wind speeds in groups of 5 m/s. As before,

$$Pr(U_{\infty i} \cap \theta_j) = \frac{N(U_{\infty i} \cap \theta_j)}{N}. \tag{3.3}$$

Table 3.5 tabulates the joint probabilities of wind speed and wind direction as a percent. For example, the highest joint probability is wind speed between 5–10 m/s while the wind is simultaneously from the south in 30° sector. This coincidence has a 14.5% chance of occurrence.

Table 3.5. Probability as a percent (joint distribution) of wind speed and wind direction combinations at hub height.

	0±15	30±15	60±15	90±15	120±15	150±15	180±15	210±15	240±15	270±15	300±15	330±15
0–5	1.8	2.0	2.5	2.6	3.7	4.5	3.9	2.7	2.2	1.6	1.6	1.9
5–10	2.7	4.1	3.8	2.7	1.3	3.0	14.5	11.9	5.9	3.3	2.6	2.0
10–15	1.1	1.4	0.5	0.2	0.0	0.1	2.8	1.7	0.9	0.8	0.6	0.2
15–20	0.2	0.2	0.0	0.0	0.0	0.0	0.1	0.1	0.1	0.1	0.2	0.1

3.6 Correlation of Atmospheric Quantities for Time of Day Tests

For any month of interest, the time of day for testing in various atmospheric stability conditions will change. Figure 3.36 shows the number of occurrences of stability conditions for all 12 months as a function of time of day. For example, neutral conditions in January most commonly occur at 16:00 local time whereas in June 20:00 is the most likely time for neutral stability conditions. These trends show that the sun is creating more mixing and increasing atmospheric turbulence, as shown in Figure 3.37. As expected, neutral condition frequency is well correlated with sunrise and sunset. The relation of stability to turbulence levels and ultimately represented by the velocity profile is shown in Figure 3.38 as well, with monthly dependence on time of day trends.

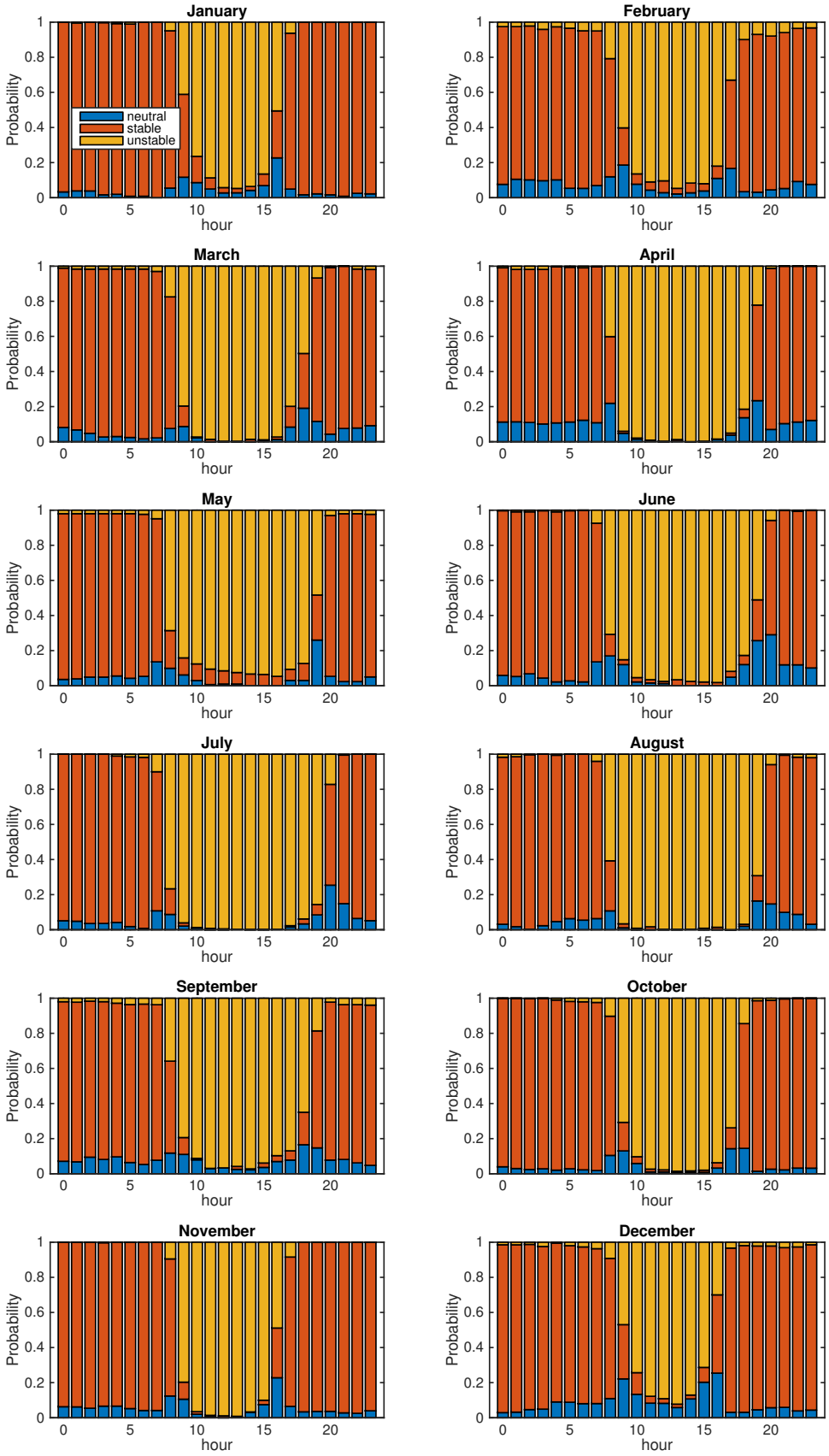

Figure 3.36. Probability of stability in the average month for each hour of the day, [3,20] m/s.

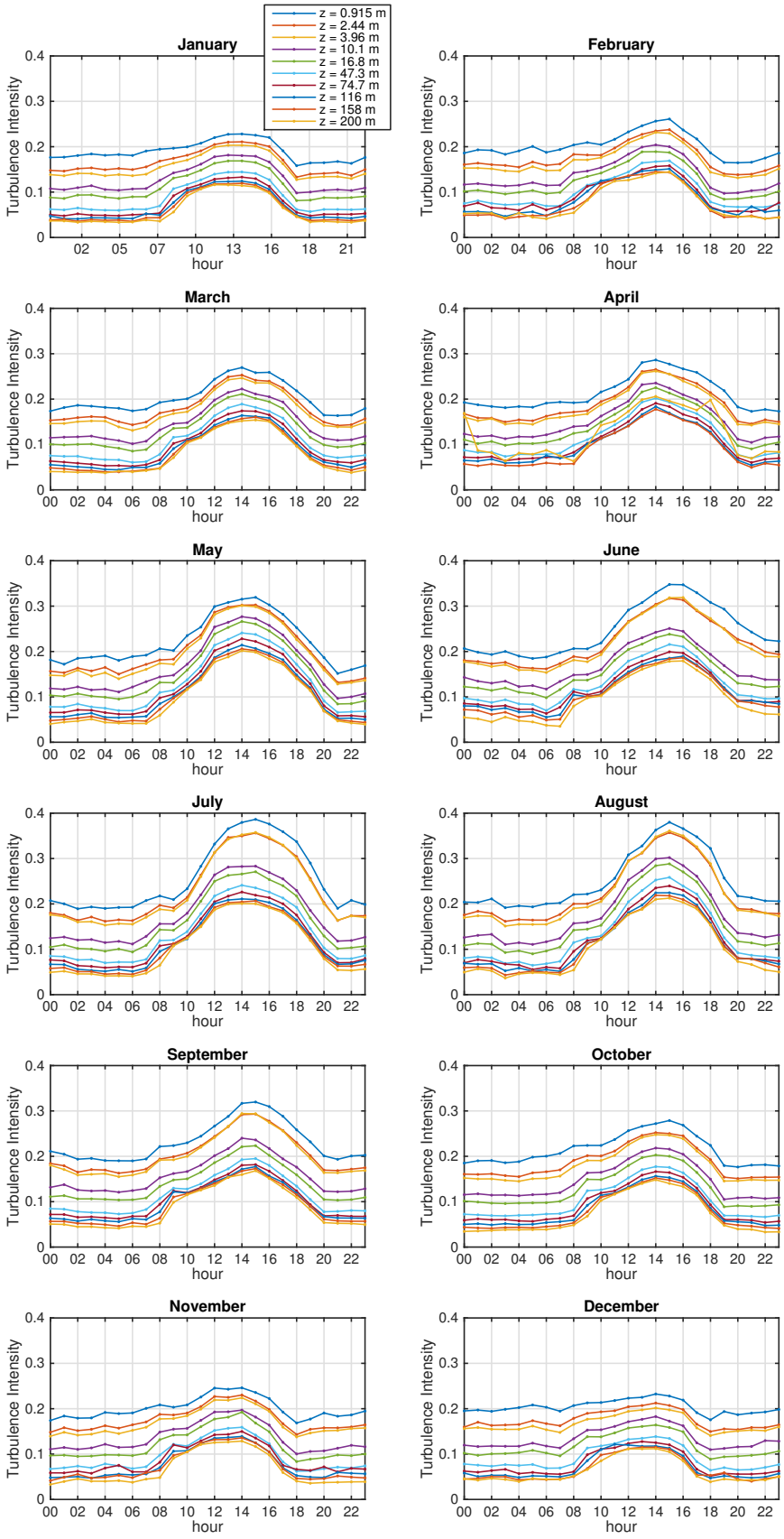

Figure 3.37. Turbulence intensity in the average month for each hour of the day, [3,20] m/s.

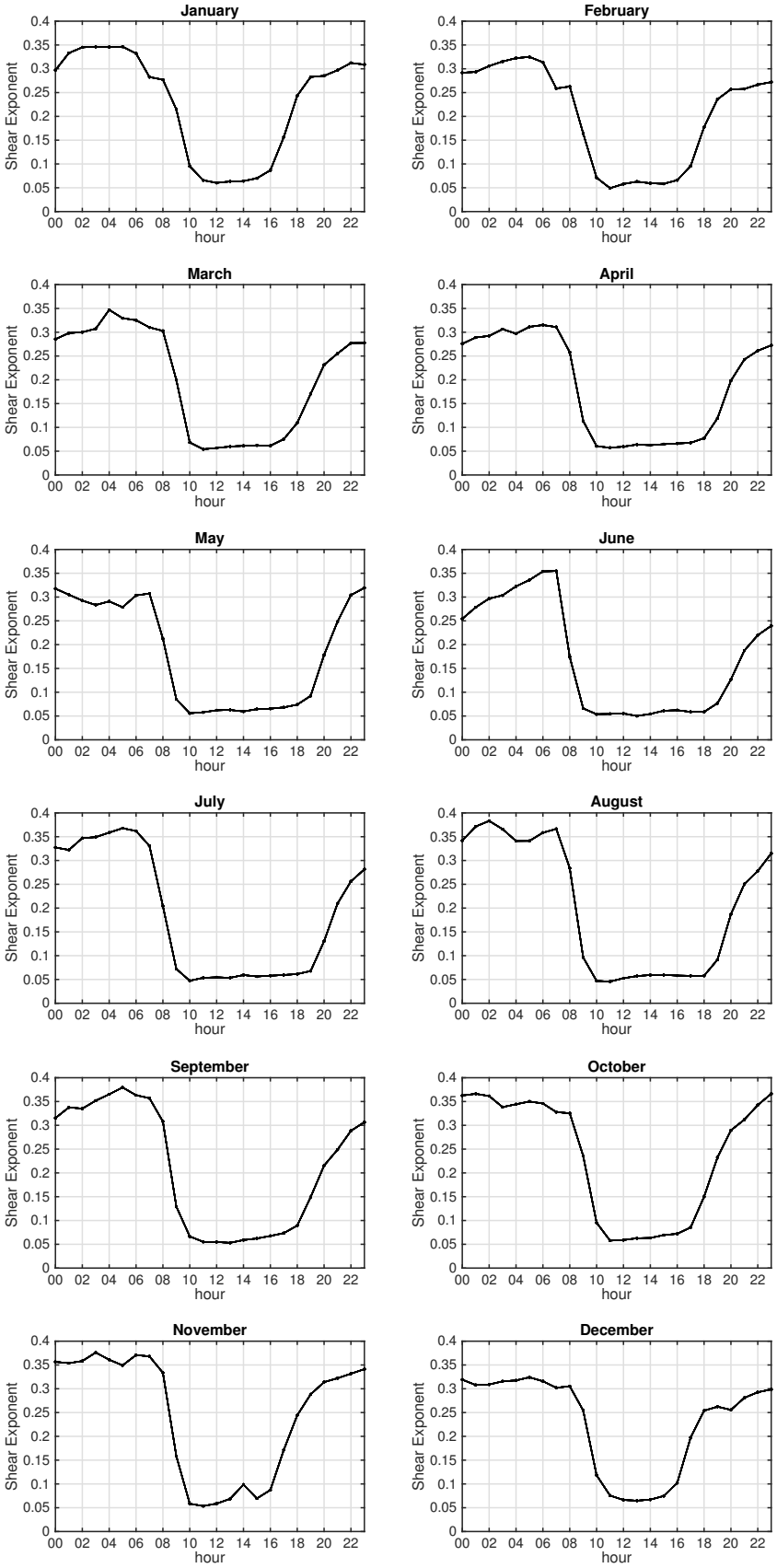

Figure 3.38. Power law profile in the average month for each hour of the day, [3,20] m/s.

Conclusions

A few major findings of the wind resource analysis of the 200 m meteorological tower at SWiFT are now summarized. The mean wind speed at hub height is 6.8 m/s, with an average turbulence intensity of 12% within the SWiFT turbine operating wind speed range. The IEC classification of the SWiFT machines is III-C. The average air density is 1.08 kg/m^3, with a large $\pm$10% fluctuation on the year.

The site is significantly directional with the wind sector of incoming wind from 160°–230° containing approximately 40% of the data. The average months in the year show the strongest trends in wind direction. June–September are the best months for 5 diameter turbine-turbine interaction experiments for winds directly from the south. June–September will also have the highest turbulence. Joint probabilities showed that winds between 5-10 m/s occurring simultaneously for wind directions between 180°$\pm$15° occur most frequently at 14% of the time.

The boom arms holding anemometers were mounted at a position to minimize the frequency at which they see waked flow from the meteorological tower. Wind from 110° to 155° is where the sensors measure incorrectly due to the tower wake, which corresponds to around 9% of the data.

The data were analyzed from daily (hour of the day) and seasonal (month of the year) perspectives with trends identified. The sun, and hence hour of the day dictates the atmospheric stability stronger than months in a year, although the percentage of stable conditions increases to 65-70% in winter from around 45% in summer. Neutral conditions occur most often on the year during two-hour windows, from 08:00–10:00 and 18:00–20:00 local time (UTC-06:00.) Stable conditions occur most at night, 20:00–07:00, and unstable conditions during late morning and afternoon, 10:00–18:00. These typical stability transition times were seen to change significantly with time of year where the amount and time of sunlight varies. Turbulence intensity is highly correlated with stability, and typical daytime unstable conditions see 18% turbulence intensity versus that experienced during the average stable night of 9%.

Velocity profile veer is preferential at this site to a clockwise increase in direction with height. Values of up to 5° are common and the higher values typically occur with stable atmospheric conditions. The high veer magnitude is typically associated then with high levels of shear and low levels of turbulence intensity, as would be expected.

This page intentionally left blank.

References

[1] Brian Hirth, J. S., "A Summary of the National Wind Institute Meteorological Measurement Facilities at the Texas Tech University's Reese Technology Center Field Site," Tech. rep., Texas Tech University, 2014.

[2] Huug G. Ouwersloot, Stephan R. de Roode, F. C. B. and Kroon, P. S., "Vertical Wind Velocity Observations from the Cabauw Tower," Tech. rep., Delft University of Technology.

[3] *IEC 61400-1 Ed.3: Wind turbines - Part 1: Design Requirements*, 2005.

[4] Jonathan Berg, Josh Bryant, B. L. D. M. B. N. J. P. B. R. J. W. D. K., "Scaled Wind Farm Technology Facility Overview," 2014.

[5] Clifton, A., "135-m Meteorological Masts at the National Wind Technology Center: Instrumentation, Data Acquisition and Processing," Tech. rep., National Renewable Energy Laboratory, 2014.

[6] Kevin Walter, Christopher C. Weiss, A. H. S. J. C. N. D. K., "Observations of Extreme Speed and Directional Wind Shear in the U.S. Great Plains," 2007.

DISTRIBUTION:

1 MS 0899 Technical Library, 9536 (electronic copy)

Sandia National Laboratories